

A least-square radial point collocation method for adaptive analysis in linear elasticity

Bernard B.T. Kee^{a,*}, G.R. Liu^{a,b}, C. Lu^c

^a*Department of Mechanical Engineering, Centre for Advanced Computations in Engineering Science (ACES), National University of Singapore, 10 Kent Ridge Crescent, Singapore 119260, Singapore*

^b*The Singapore-MIT Alliance (SMA), E4-04-10, 4 Engineering Drive 3, Singapore 117576, Singapore*

^c*Institute of High Performance Computing (IHPC), 1 Science Park Road, #01-01, The Capricorn, Singapore Science Park II, Singapore 117528, Singapore*

Received 10 October 2007; accepted 18 November 2007

Available online 22 January 2008

Abstract

This paper presents a least-square radial point collocation method (LS-RPCM) that is formulated based on the strong formulation and the local approximation using radial basis functions (RBFs). Aiming to solve the instability problem observed in the conventional RPCM using local nodes, a simple and yet effective procedure that uses the well-known least-square technique in a carefully designed manner has been proposed to restore the stability. Since stable solution can now be obtained, the LS-RPCM is then extended for adaptive analysis. Attractive features of the meshfree strong-form method that facilitate the implementation of adaptive analysis are demonstrated via a number of examples in this work. A robust residual based error estimator and a simple refinement procedure using Delaunay diagram are adopted in our adaptive scheme. Stable and accurate results are obtained in all the numerical examples.

© 2007 Elsevier Ltd. All rights reserved.

Keywords: Meshfree method; Strong formulation; Radial basis function; Adaptive analysis; Residual; Error estimator; Delaunay diagram

1. Introduction

Following the great success of the finite element method, a new class of computational methods, meshfree methods, has been drawing much attention from researchers in the recent decades. Unlike the finite element method, the meshfree method is “free” from the mesh in shape function constructions, and is becoming a promising computational method.

The earliest work of the meshfree method can be traced back to 1970s; Lucy and Monaghan introduced smoothed particle hydrodynamics (SPH) method to solve astronomic problems [1–3]. Since then many meshfree methods have been proposed, intensive reviews and thorough studies on the development of the meshfree methods are abundantly available in the literature [3–6]. According to the formulation procedures, meshfree methods can be categorized into

three major groups [6]. The first group of meshfree methods is formulated based on the strong formulation known as the meshfree strong-form method. Typical meshfree strong-form method may include smoothed particle hydrodynamics (SPH) method [1–3], diffusion approximation method (DAM) [52], finite point method (FPM) [8,51], hp-meshless cloud method [9], general finite different method (GFDM) [10–14,55], radial point collocation method (RPCM) [6,15], etc. The second group of meshfree method is formulated based on the weak formulation, namely the meshfree weak-form method. Majority of the meshfree methods belong to this group, for instance, meshless local Petrov–Galerkin (MLPG) method [16], element-free Galerkin (EFG) method [17], reproducing kernel particle method (RKPM) [18], local radial point interpolation method (LRPIM) [19,20], point interpolation method [21,22], radial point interpolation method [23,53], etc. Some of the meshfree weak-form methods are however not regarded as “true” meshfree method as background mesh is still necessary in their formulation. The last group of meshfree method is

*Corresponding author.

E-mail addresses: g0301110@nus.edu.sg (B.B.T. Kee),
mpeliugr@nus.edu.sg (G.R. Liu), luchun@ihpc.a-star.edu.sg (C. Lu).

formulated based on both strong and weak formulations, or known as the meshfree weak–strong (MWS) forms method [25,26]. In the MWS formulation, the strong-form formulation (collocation) is applied to all the internal nodes and nodes on the Dirichlet boundaries, and the local weak formulation is *only* applied on the Neumann boundary.

Among these three groups of meshfree methods, the weak-form method is the most well-established method due to the use of the variational principle that provides good stability. In contrast, the development of the meshfree strong-form method is rather sluggish. Available literature for the meshfree strong-form method using local nodes is very limited. Nevertheless, the meshfree strong-form method possesses many good features. It is regarded as a truly meshfree method as it does not even require a background mesh, because no integration is needed in the formulation. Such distinct feature facilitates the implementation of the refinement or coarsening scheme in the adaptive analysis as node can be easily inserted or removed without worrying too much about the nodal connectivity. It is obvious that the strong formulation is much simple, straightforward and easy to implement. Apparently, the meshfree strong-form method is a better candidate for adaptive analysis compared to the meshfree weak-form method. Some research works of meshfree strong-form method for adaptive analysis have been reported in the literature [6,27–29].

Currently, most reliable strong-form methods are still very much relying on the structure grids and restricted only for regular domain. Finite difference method (FDM) is considered as the most classical, reliable and earliest strong-form method [30]. However, while dealing with more geometrically complex and practical problems, the FDM that relies on the structure grids has encountered great difficulty. A strong-form meshfree method that is formulated without relying on the structure grid is therefore very attractive. Although method like GFDM [12–16] claims that it can be used for irregular domain and unstructured grids, a proper stencil (nodal selection) is somehow still needed for function approximation. The cumbersome procedure of nodal selection constrained the strong-form method from being used in the adaptive process as nodal distribution during the adaptation can be highly irregular and hence results in difficulties in forming the “proper” stencils.

Recently, radial basis functions (RBFs) have been broadly used in the meshfree method for constructing the shape functions. As RBFs are well known for their excellence performance in scattered data fitting, the strong-form method that is based on RBFs can work very well with irregular grids. Kansa is the first to adopt RBFs in collocation method for solving partial differential equations (PDEs) [31] using all the nodes in the problem domain for “one-piece” interpolation. The coefficient matrix constructed by the conventional RBFs scheme using “global” nodes for one-piece interpolation is a full

matrix, and results in poor conditioning and low accuracy in the solution [32]. Several techniques include domain decomposition [32], RBFs with compact support [33], adding fictitious nodes [34] and modified Kansa method [35] with double use of the boundary nodes have been introduced to improve the conditioning of the coefficient matrix and the solution accuracy.

To overcome the ill-conditioning of the full coefficient matrix, a novel idea that can construct a banded coefficient matrix is the key to develop a practical meshfree strong-form method that is competitive to the weak-form methods. Such new RBFs scheme that is based on local nodes and piecewise interpolation known as the RPCM has been therefore suggested [6,17,28,36,37]. Other recent works have also been presented using local nodes and piecewise interpolation in the function approximation [38,39]. The work presented in this paper will be based on the RPCM, where RBFs approximation is used to construct the shape functions using only local nodes and piecewise interpolation.

The instability problem is another crucial issue that limits the application of strong-form method that uses local nodes, especially in the adaptive analyses. Without an effective stabilization measure, it is impossible to use such a meshfree strong-form method for adaptive analyses. Researchers have also introduced several stabilization schemes [8,28,29]; however, stabilization factor has to be determined or special treatment is needed in those works. The idea of using least-square technique to solve strong-form collocation method is a natural choice. Zhang et al. has proposed to use a least-square formulation [40] with some auxiliary points in the domain; however, their formulation is based on global nodes and one-piece interpolation.

The author believes that a comprehensive and insightful study on the root of the instability problem is very important to develop effective techniques to overcome the stability problem in the strong-form meshfree methods which use local nodes for piecewise function approximation. From a large number of numerical investigations, we observed the strong-form solution oscillates heavily on the boundary of the problem domain when the RPIM shape functions created using local nodes. We believe that such oscillation is caused by the “strong” requirement for the approximated field variable to satisfy governing equations and boundary conditions “exactly” at all the nodes. Based on our observation and understanding on the oscillation phenomenon, a novel and simple least-square RPCM (LS-RPCM) is proposed based on the strong formulation. In this formulation procedure, additional collocation points are *only* inserted on the boundary. A common technique, least-square technique, is then adopted to provide certain “relaxation” effect upon the strong formulation. The oscillation phenomenon will be illustrated in detail in the following sections and in the numerical examples.

Our intensive numerical study will also demonstrate that a stable and accurate solution can be obtained from the

present procedure. Furthermore, the LS-RPCM is also successfully implemented for adaptive analyses. Compared with other existing strong-form methods, nodal selection in the LS-RPCM is much more flexible. The present formulation of the LS-RPCM remains simple, straightforward and no integration is needed. The great stability and advantages of the LS-RPCM are well demonstrated in the numerical examples of adaptive analysis.

In our adaptive analysis, a residual based error estimator is devised and used in this work. By evaluating the residual of the governing equations in the domain, the error estimator can effectively identify the critical regions to be refined during adaptation. In general, the refinement schemes can be classified into three major categories, which are *h*-refinement, *p*-refinement and *r*-refinement schemes. The details of the procedure for different refinement schemes can be found in Ref. [41]. In this work, *h*-refinement is adopted our adaptive scheme. Unlike the conventional *h*-refinement scheme in which mesh is enriched, additional nodes are inserted into the domain based on the error estimator in our *h*-refinement procedure. The Delaunay diagram is introduced to locate the position of the additional nodes to be inserted into the domain. As long as meshfree strong-form method is concerned, additional nodes can be inserted into the domain without worry of the nodal connectivity.

2. Function approximation

In the present formulation, RBF augmented with polynomial function is used to approximate the field functions and its derivatives. The RBFs have been widely used for scattered data fitting in the mathematic community [42,43]. In early 1990s, Kansa used RBFs for solving PDEs [31]. Since then RBFs are well discussed and many research works have been followed up [44–46]. In Kansa’s

Table 1

Typical generalized radial basis functions [4,5], where $r_i = \|\mathbf{x} - \mathbf{x}_i\|$ is the Euclidian norm in the vector space

Type	Expression	Dimensionless Shape Parameter
Multi-quadrics (MQ)	$R_i(x, y) = (r_i^2 + (\alpha_c d_c)^2)^q$	α_c, q
Gaussian (EXP)	$R_i(x, y) = \exp(-cr_i^2)$	C
Thin plate spline (TPS)	$R_i(x, y) = r_i^\eta$	η
Logarithmic	$R_i(x, y) = r_i^\eta \log r_i$	η

The shape parameters are arbitrary real numbers.

matrix can be effectively avoided. There are many RBFs available in the literature, typical generalized RBFs with arbitrary real shape parameters [5,6] listed in Table 1 are found in great performance.

Consider an unknown field function $u(\mathbf{x})$ that can be approximated in the vicinity of an interest point \mathbf{x} in the problem domain by the local radial point interpolation in the following form as

$$u^h(\mathbf{x}) = \sum_{i=1}^n a_i r_i(\|\mathbf{x} - \mathbf{x}_i\|) + \sum_{j=1}^m b_j p_j, \tag{1}$$

where n is the total number of the supporting nodes in the local domain, m is the number of the monomials in the polynomial function, $r_i(\|\cdot\|)$ is the radial basis function and p_j is the monomial in the polynomial function for augmentation. a_i and b_j are the coefficients of the radial basis function and the monomial of the polynomial function.

By enforcing the interpolation passing through the nodal values at the local nodes, the following expression can be obtained,

$$\begin{bmatrix} u_1 \\ u_2 \\ \vdots \\ u_n \end{bmatrix} = \begin{bmatrix} r_1(\|\mathbf{x}_1 - \mathbf{x}_1\|) & r_1(\|\mathbf{x}_1 - \mathbf{x}_2\|) & \cdots & r_1(\|\mathbf{x}_1 - \mathbf{x}_n\|) & p_1(\mathbf{x}_1) & \cdots & p_m(\mathbf{x}_1) \\ r_2(\|\mathbf{x}_2 - \mathbf{x}_1\|) & r_2(\|\mathbf{x}_2 - \mathbf{x}_2\|) & \cdots & r_2(\|\mathbf{x}_2 - \mathbf{x}_n\|) & p_1(\mathbf{x}_2) & \cdots & p_m(\mathbf{x}_2) \\ \vdots & \vdots & \ddots & \vdots & \vdots & \ddots & \vdots \\ r_n(\|\mathbf{x}_n - \mathbf{x}_1\|) & r_n(\|\mathbf{x}_n - \mathbf{x}_2\|) & \cdots & r_n(\|\mathbf{x}_n - \mathbf{x}_n\|) & p_1(\mathbf{x}_n) & \cdots & p_m(\mathbf{x}_n) \end{bmatrix} \begin{bmatrix} a_1 \\ \vdots \\ a_n \\ b_1 \\ \vdots \\ b_m \end{bmatrix}$$

works, as all nodes in the problem domain are used for the function approximation, the full coefficient matrix is usually with large condition number [32].

Recently, a function approximation based on “local” radial point interpolation piecewisely has been well discussed in both strong [17,36,37] and weak [19,20,23,24] formulations. In these works, the “local” radial point interpolation is used: only vicinity nodes are involved for the local function approximation in a piecewise manner. With such a local radial point interpolation, full coefficient

or in concise form

$$\mathbf{U} = [\mathbf{R} \quad \mathbf{P}] \begin{bmatrix} \mathbf{a} \\ \mathbf{b} \end{bmatrix}, \tag{2}$$

where \mathbf{U} is the vector of unknown nodal values, \mathbf{a} and \mathbf{b} are the vector of coefficients of the radial basis functions and the monomials of the polynomial function, respectively.

With the orthogonal condition [32,42],

$$\mathbf{P}^T \mathbf{a} = 0, \tag{3}$$

a unique vector of coefficients can be obtained as

$$\begin{bmatrix} \mathbf{a} \\ \mathbf{b} \end{bmatrix} = \begin{bmatrix} \mathbf{R} & \mathbf{P} \\ \mathbf{P}^T & 0 \end{bmatrix}^{-1} \begin{Bmatrix} \mathbf{U} \\ 0 \end{Bmatrix} = \mathbf{G}^{-1} \begin{Bmatrix} \mathbf{U} \\ 0 \end{Bmatrix}. \quad (4)$$

The unknown approximated field function $u(\mathbf{x})$ at interest point \mathbf{x} can then be expressed as

$$u^h(\mathbf{x}) = [\phi_1(\mathbf{x}) \ \phi_2(\mathbf{x}) \ \cdots \ \phi_n(\mathbf{x})]\mathbf{U} = \Phi(\mathbf{x})\mathbf{U}, \quad (5)$$

where $\phi(\mathbf{x})$ is the shape function called RPIM shape function. The derivatives of the field function can be easily obtained by differentiating the shape functions. For example, the first derivative of the field function with respect to k can be expressed as

$$u_{,k}^h(\mathbf{x}) = \Phi_{,k}(\mathbf{x})\mathbf{U}. \quad (6)$$

The details of constructing the RPIM shape function and its other properties can be found in, e.g. Refs. [5,6].

Note that Eq. (5) gives a piecewise approximation of the field function u in the vicinity of the point of interest \mathbf{x} . The point \mathbf{x} can be any point in the problem domain: at nodes or otherwise. Where \mathbf{x} changes, the local nodes will be changed accordingly. Using this piecewise approximation of Eq. (5), a simple collocation procedure can be easily used to create a set of algebraic equations that can be solved using standard solver, if the equations well behaved. In usual situation, these equations obtained by simple collocations do not behave well, and hence technique present in this work is needed to establish a set of equations that are stable and well behaved.

In this paper, multiquadrics (MQ) and completed second-order polynomial, $m = 6$, are used in the function approximation. In the MQ-RBF, two dimensionless shape parameters that have great influence to the accuracy are needed to be determined. However, by augmenting the polynomial function with the RBFs, the effects of dimensionless shape parameters to the RBFs can be reduced [24]. In this work, we adopt the recommended values reported by Liu and co-workers [5,6,24] for the shape parameters used for MQ are adopted from the: $\alpha_c = 3.0$ and $q = 1.03$.

Note that the nodal selection for the radial point interpolation should be forming at least a “layer” of nodes surround the interpolation point \mathbf{x} . For instance, in one-dimensional case, the supporting nodes must at least include one node on both sides of the interpolation point as shown in Fig. 1. To ensure \mathbf{G} in Eq. (4) is invertible, the number of supporting nodes has to be at least equal to the number of the monomials used in the polynomial function, $n \geq m$. In our work, the number of supporting nodes is about two to three times of the number of the monomials, $n = 2 - 3m$. (7)

3. Radial point collocation method

Consider a problem in a domain Ω is governed by the following PDEs:

$$L(u) = f \text{ in } \Omega, \quad (8)$$

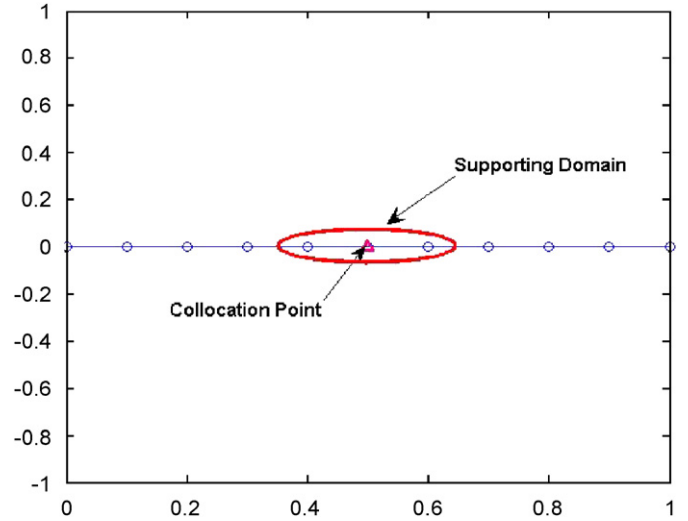


Fig. 1. Nodal selection for constructing shape function in one-dimensional space.

with Neumann boundary condition,

$$B(u) = g \text{ on } \Gamma_t, \quad (9)$$

and Dirichlet boundary condition,

$$u = \bar{u} \text{ on } \Gamma_u, \quad (10)$$

where $L(\cdot)$, $B(\cdot)$ are the differential operators and u is the field variable.

In the conventional collocation method, the above governing equation and boundary conditions are simply collocated at their corresponding field nodes, respectively, as follows:

$$L(u_i) = f_i \text{ in } \Omega, \quad (11)$$

with Neumann boundary condition,

$$B(u_i) = g_i \text{ on } \Gamma_t, \quad (12)$$

and Dirichlet boundary condition,

$$u_i = \bar{u}_i \text{ on } \Gamma_u, \quad (13)$$

where subscript “ i ” denotes the collocation point.

The discretized system equations can then be assembled and expressed in the following matrix form as

$$\mathbf{K}\mathbf{U} = \mathbf{F}, \quad (14)$$

where \mathbf{K} denotes the coefficient matrix, \mathbf{F} denotes the force vector and \mathbf{U} is the vector of unknown nodal field values. Note that the coefficient matrix of the collocation method is generally unsymmetric. The vector of unknown nodal values can be easily solved as

$$\mathbf{U} = \mathbf{K}^{-1}\mathbf{F}, \quad (15)$$

if \mathbf{K} is not singular and well conditioned.

4. Least-square procedure

Studies (e.g. [6]) have found that \mathbf{K} given in Eq. (15) obtained by simple collocation is not usually not well

conditioned, and such a strong-form method can provide unstable solution. Therefore, it is difficult to use them in an adaptive analysis. In this work, we propose a simple and yet effective procedure, least-square procedure, to obtain stable solutions.

Through our observation, Neumann boundary condition is the cause of the instability. We found that the conventional RPCM performs well for solving one-dimensional problem and Dirichlet problem. However, the solution of conventional RPCM becomes unstable while dealing with Neumann boundary condition. Oscillation phenomenon is observed on the boundary. It could be due to the “strong” requirement of satisfaction of the Neumann boundary condition in the strong formulation. To provide a kind of “relaxation” effect, least-square approach is a natural choice to be adopted.

In the present formulation, additional collocation points are added on the boundary and allocated in between the boundary nodes as shown in Fig. 2. The Neumann and Dirichlet boundary conditions in Eqs. (12) and (13) can be collocated at the additional collocation points on the boundary, respectively. The additional algebraic equations can be assembled and expressed in the matrix form as follows:

$$\begin{bmatrix} \mathbf{K}_{N'} \\ \mathbf{K}_{D'} \end{bmatrix} \mathbf{U} = \begin{bmatrix} \mathbf{F}_{N'} \\ \mathbf{F}_{D'} \end{bmatrix} \quad \text{or} \quad \mathbf{K}_a \mathbf{U} = \mathbf{F}_a, \quad (16)$$

where $\mathbf{K}_{N'} \mathbf{U} = \mathbf{F}_{N'}$ and $\mathbf{K}_{D'} \mathbf{U} = \mathbf{F}_{D'}$ are the additional sets of algebraic equations for additional collocation points on the Neumann and Dirichlet boundaries, respectively. Augmented the additional algebraic equations to the original system equations, one can obtain an “over-posed” problem [47]:

$$\begin{bmatrix} \mathbf{K} \\ \mathbf{K}_a \end{bmatrix} \mathbf{U} = \begin{bmatrix} \mathbf{F} \\ \mathbf{F}_a \end{bmatrix} \quad \text{or} \quad \tilde{\mathbf{K}} \mathbf{U} = \tilde{\mathbf{F}} = 0. \quad (17)$$

As the number of algebraic equations is more than the number of unknown variable \mathbf{U} , a common least-square technique using QR-algorithm is applied to solve for the

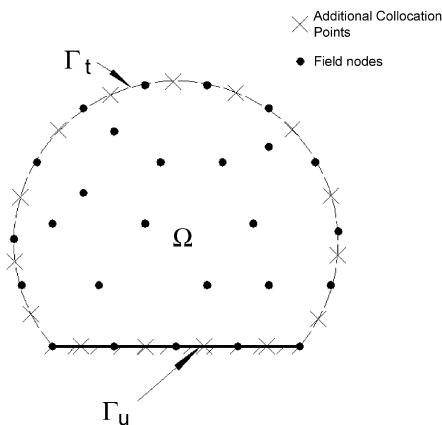


Fig. 2. Field nodes and additional collocation points in a problem domain and boundaries.

vector of unknowns \mathbf{U} by minimizing the residual in Eq. (17). Before the set of equations is solved, to have equal weight for each algebraic equation, each equation should be normalized by the value of the largest entry in the corresponding row of the coefficient matrix $\tilde{\mathbf{K}}$. The normalized algebraic equations can be expressed in the following matrix form,

$$\hat{\mathbf{K}} \mathbf{U} = \hat{\mathbf{F}}, \quad (18)$$

where $\hat{\mathbf{K}}$ denotes the normalized coefficient matrix and $\hat{\mathbf{F}}$ denotes the normalized force vector. In the conventional RPCM, although the boundary conditions are fully satisfied at the boundary nodes, stable solution cannot be ensured. From our study [25,28,29], the cause of instability could be due to the imposition of Neumann boundary condition. We believe that by introducing more collocation points along the boundary, the least-square procedure can provide certain “relaxation” upon the strong formulation and hence a more stable solution can be obtained. The key point of the least-square procedure is that having additional collocation points along the boundary is enough to stabilize the solution. Introducing additional collocation points in the internal domain may help but it is not necessary. This is in line with the principle of the MWS method [25,26].

5. Adaptive scheme

As the RPCM is a truly meshfree method, it possesses attractive features to facilitate an easier implementation for adaptive scheme. Without the constraint of the nodal connectivity, additional nodes can be inserted during refinement process easily. Cumbersome remeshing process is also avoided.

A good error estimator plays a very important role in the adaptive analysis. In our adaptive scheme, a robust error

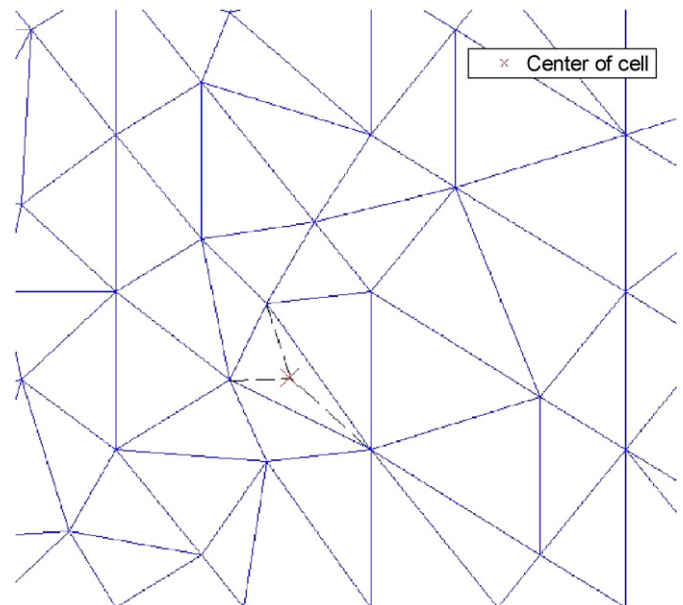


Fig. 3. Residual evaluated at the middle of the Delaunay cell.

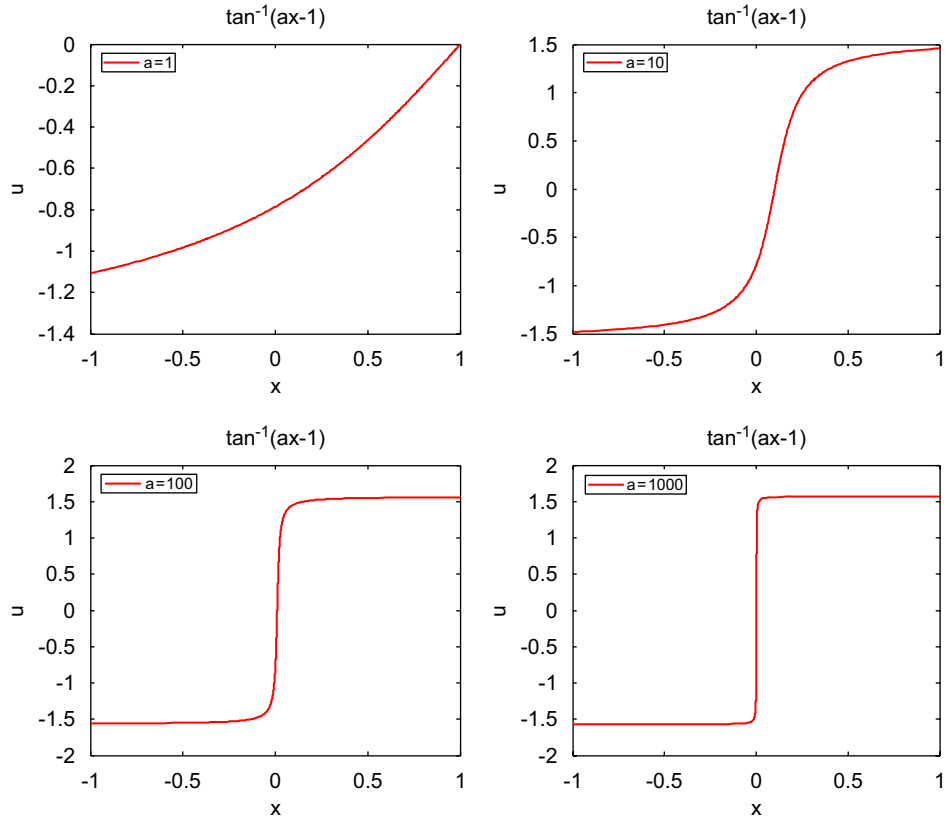


Fig. 4. Exact solution of field function u for different gradient a .

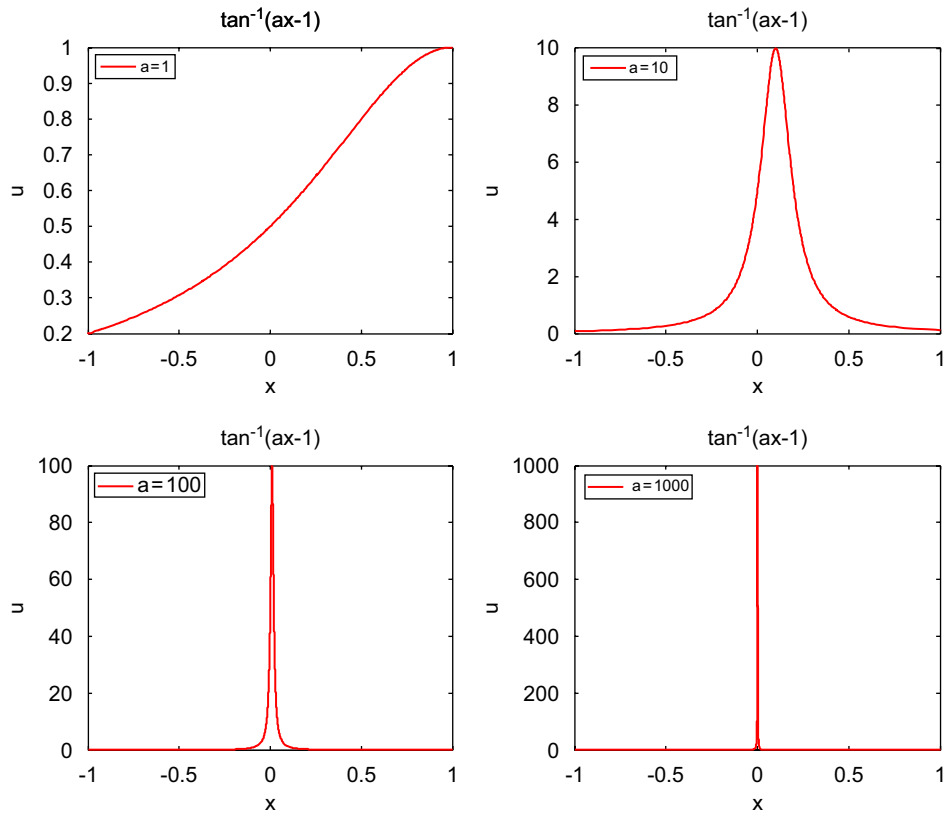


Fig. 5. Exact solution of the first derivative of field function u for different gradient a .

estimator based on residual of the governing equation is adopted. The residual based error estimator provides a good measurement for the quality of the local approximation and the global accuracy of the solution. The details of the error estimator and refinement procedures are given as follows.

5.1. Error estimator

In our adaptive scheme, the problem domain is first represented using Delaunay diagram. The error estimator is computed by evaluating the residual of the governing equations at the centre of the Delaunay cells as shown in

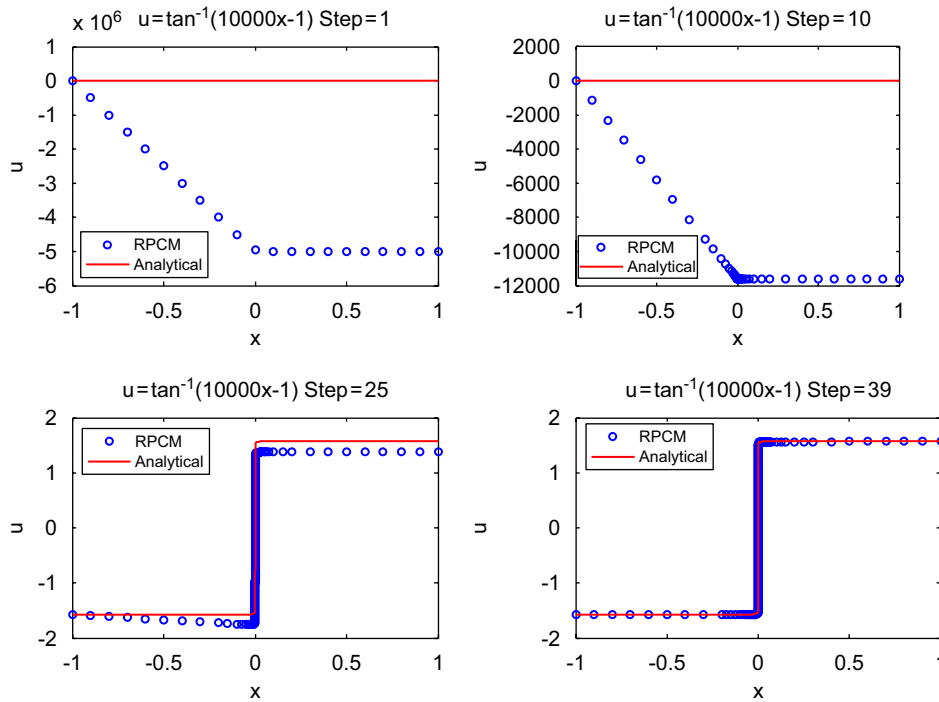


Fig. 6. The solution of field function u , at 1st, 10th, 25th and final step.

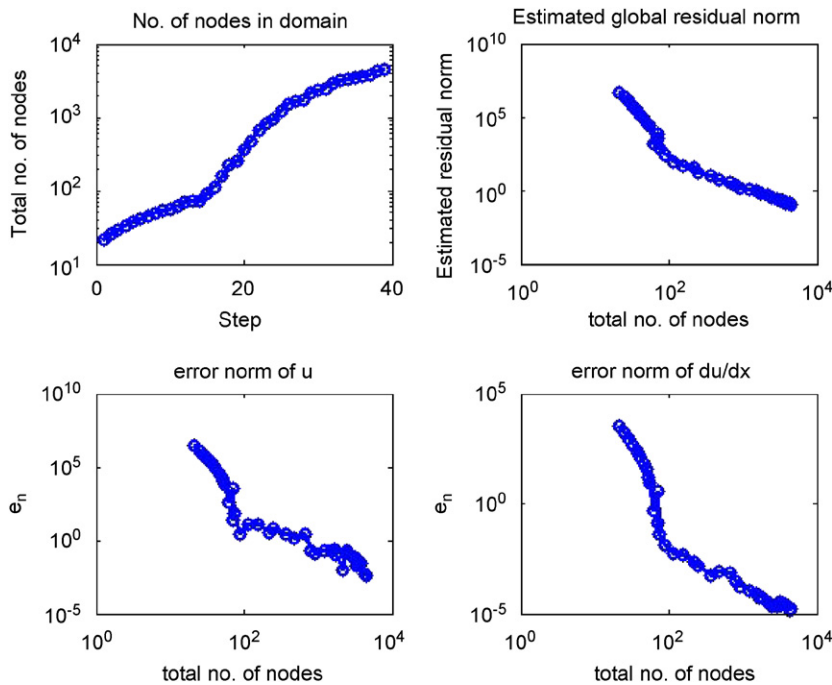


Fig. 7. The error of the field function u and its first derivative at each adaptive step.

Fig. 3. The local error estimator is defined as

$$\eta_j = \int_{\Omega_j} \|Lu - f\|_{L_2} d\Omega \approx \frac{1}{3} A_j \|Lu_j - f_j\|_{L_2}, \quad (19)$$

where A_j is the area of the j th Delaunay cell and the $\|Lu_j - f_j\|_{L_2}$ is the L_2 norm of the residual of the governing equation evaluated at the centre of the corresponding cell.

With above definition of the local error estimator, the estimated global residual norm can be easily obtained as

$$\eta_g = \sqrt{\int \|Lu - f\|_{L_2}^2 d\Omega} \approx \sqrt{\sum_{j=1}^{nc} \left[\frac{1}{3} A_j (Lu_j - f_j) \right]^2}, \quad (20)$$

where nc is the total number of Delaunay cells.

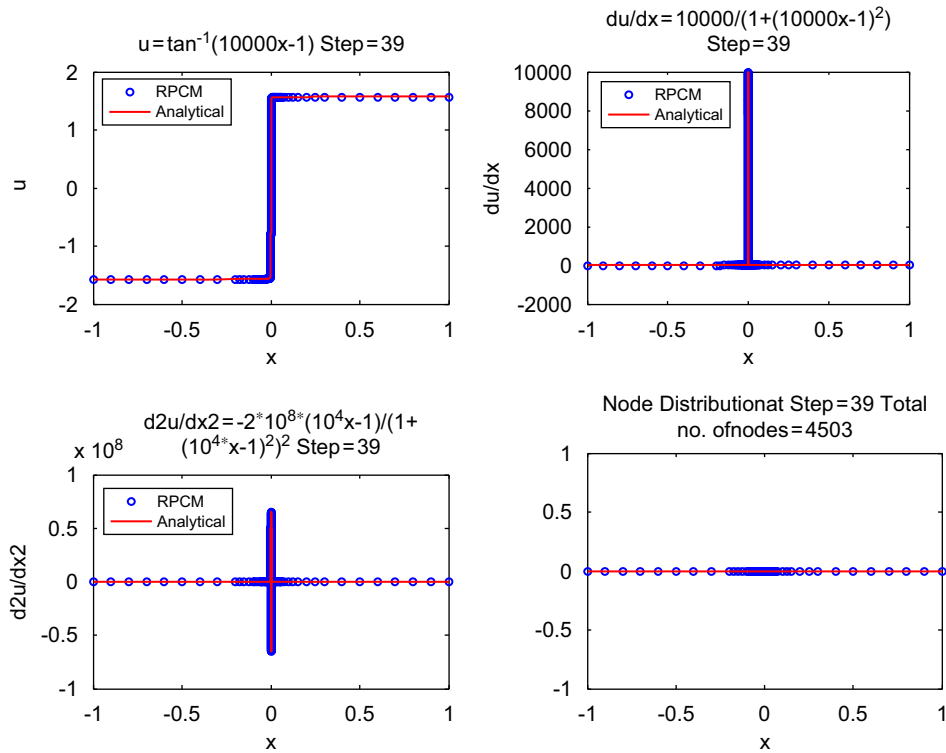


Fig. 8. The field function u , its first derivative and second derivative at the final adaptive step.

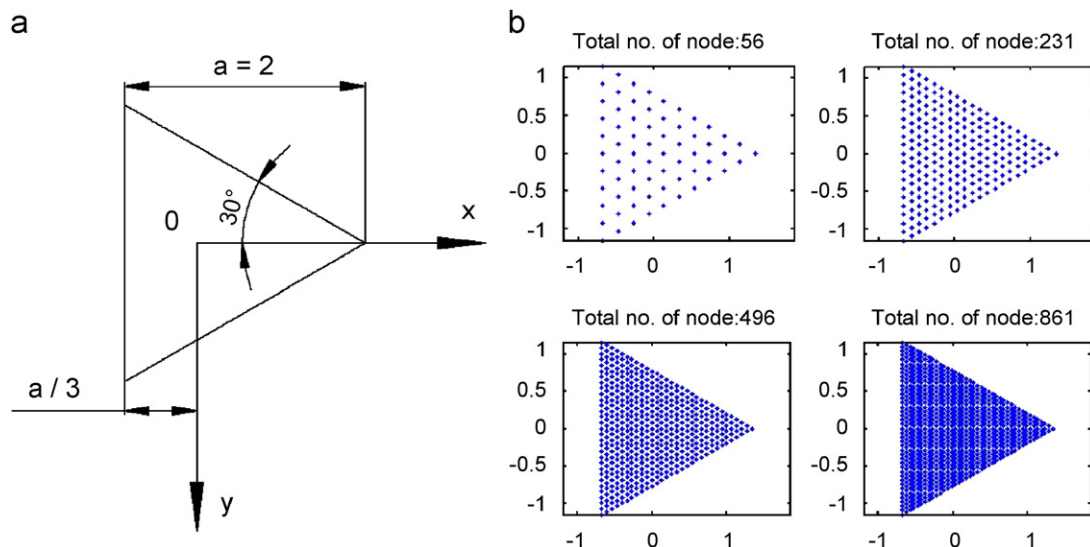


Fig. 9. (a) Dimensions of the triangular bar and (b) four sets of regular nodal distribution.

5.2. Refinement and stopping criteria

In our adaptive scheme, the refinement criteria is defined as

$$\eta_j \geq \kappa_l \eta_m, \tag{21}$$

where κ_l is the local refinement coefficient and η_m is the maximum local error estimator in the entire domain,

$$\eta_m = \max(\eta_j). \tag{22}$$

The estimated global residual norm defined in Eq. (20) is used as a stopping indicator of the adaptive process. The stopping criteria is defined as

$$\eta_g \leq \kappa_g \eta_{mg}, \tag{23}$$

where κ_g is the global residual tolerance and η_{mg} is the maximum global error estimator value throughout the adaptive process. Once the criteria is met, the adaptive process will be terminated.

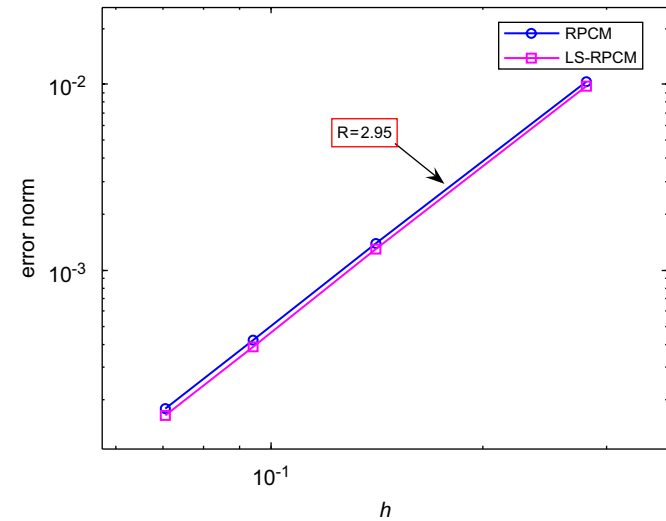


Fig. 10. Convergent rate of the solutions obtained by RPCM and LS-RPCM.

5.3. Refinement procedure

As the RPCM is a truly meshfree method, the refinement process is very simple and straightforward. Nodal can be conveniently inserted into the domain without worry of the nodal connectivity. The costly remeshing process is also not required to carry out as well. In our adaptive strategy, additional node will be inserted in the centre of the Delaunay cell if the refinement criteria (Eq. (21)) is met.

6. Numerical examples

In this paper, the norm for true error is defined as follows:

$$e = \sqrt{\frac{\sum (s^{exact} - s^{appr})^2}{\sum (s^{exact})^2}}, \tag{24}$$

where s^{exact} is the exact solution and s^{appr} numerical solution.

6.1. Example 1

In the first example, a one-dimensional Poisson problem with solution of steep gradient is studied. This example shows the excellent performance of the RPCM in adaptive

Table 2
Accuracies of the RPCM and LS-RPCM for torsion problem

No. of nodes	h (average spacing)	Error norm of RPCM	Error norm of LS-RPCM
<i>Regular nodal distribution (triangular cross section)</i>			
66	0.2807	0.0104	0.0098
231	0.1409	0.0014	0.0013
496	0.0940	4.1776e-4	3.8730e-4
861	0.0706	1.7879e-4	1.6556e-4
<i>Irregular nodal distribution (elliptic cross section)</i>			
511	0.1160	3.5847e-15	5.2227e-15

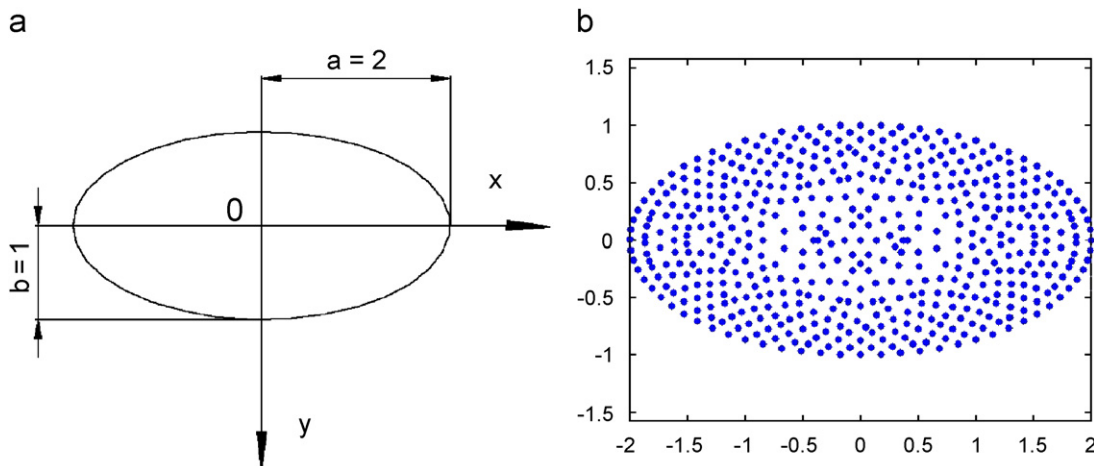


Fig. 11. (a) Dimensions of elliptic bar and (b) the model with 511 irregularly distributed nodes.

analysis. The Poisson problem governed by the following ordinary differential equation (ODE),

$$\frac{d^2u}{dx^2} = \frac{-2a^2(ax-1)}{[1+(ax-1)^2]^2}, \quad x \in \Omega : [-1, 1], \quad (25)$$

where a is a constant. Dirichlet boundary condition is imposed at left end,

$$u = \tan^{-1}(ax-1) \quad \text{at } x = -1, \quad (26)$$

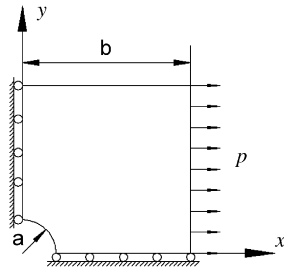


Fig. 12. Model of a plate subjected to a unit traction in the horizontal direction.

and Neumann boundary condition is imposed at right end,

$$\frac{du}{dx} = \frac{a}{1+(ax-1)^2} \quad \text{at } x = 1. \quad (27)$$

The exact solution for the above ODE is known as

$$u = \tan^{-1}(ax-1). \quad (28)$$

From the exact solution (Eq. (28)), we know that the gradient of the field function u depends on the value of the constant a . The exact solution of the field function u and its first derivative for different a are plotted in Figs. 4 and 5, respectively. In this example, an extremely large value of $a = 10^4$ is deliberately selected for the purpose of examining the robustness of the RPCM and the residual based error estimator for the Poisson problem with solution of steep gradient in one-dimensional space.

An extremely low global residual tolerance is set as $\kappa_g = 5 \times 10^{-7}$ and local refinement coefficient is preset as $\kappa_l = 0.1$. The entire analysis takes 39 steps to complete and the nodal distributions at 1st, 10th, 25th and final steps are plotted in Fig. 6.

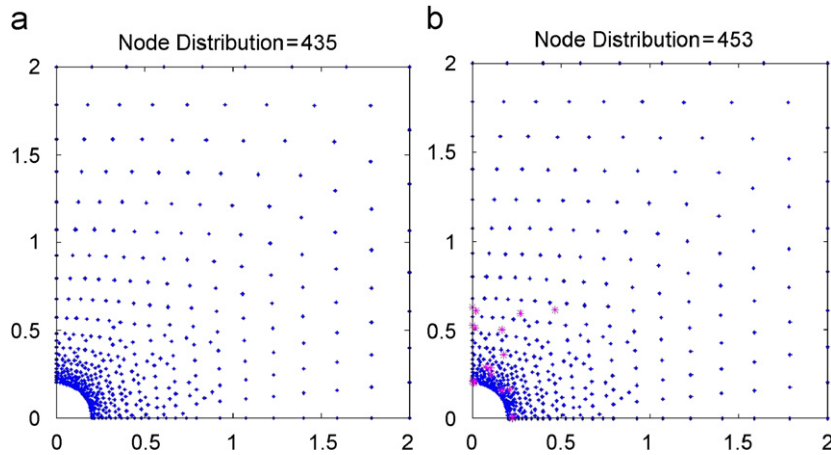


Fig. 13. Model of plate with (a) 435 nodes and (b) with additional 18 nodes to the model of 435 nodes.

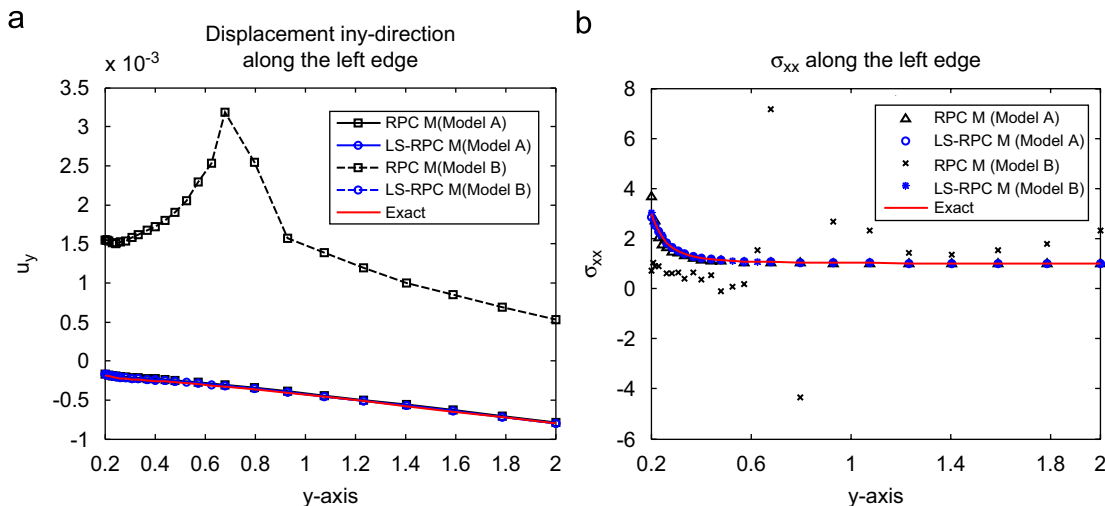


Fig. 14. (a) Displacement in y -direction and (b) normal stress σ_{xx} along the left edge for Models A and B.

The results of the adaptive analysis using the RPCM are given in Fig. 7. The estimated global residual norm and the error of the solution have been tremendously reduced through our adaptive scheme. One can observe that the adaptive RPCM is able to capture and refine the high gradient region. Majority of the nodes have been inserted

at the high gradient region as shown in Figs. 6 and 8. The numerical solutions for the field function and its gradient are greatly improved by our adaptive approach. The residual based error estimator is also shown robust in this example. Stable and accurate results are obtained by our adaptive scheme.

6.2. Example 2

In the second example, a two-dimensional torsion problem is studied. We consider a uniform bar that is twisted by couples applied at the ends [48]. The equilibrium equation of the torsion problem can be expressed as

$$\frac{\partial^2 \varphi}{\partial x^2} + \frac{\partial^2 \varphi}{\partial y^2} = -2G\theta, \tag{29}$$

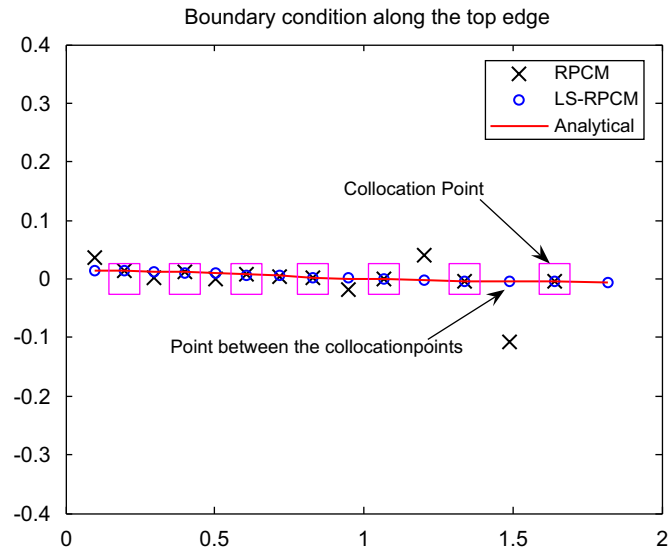


Fig. 15. Normal stress σ_{yy} along the top edge: the result obtained using RPCM is oscillating on the boundary.

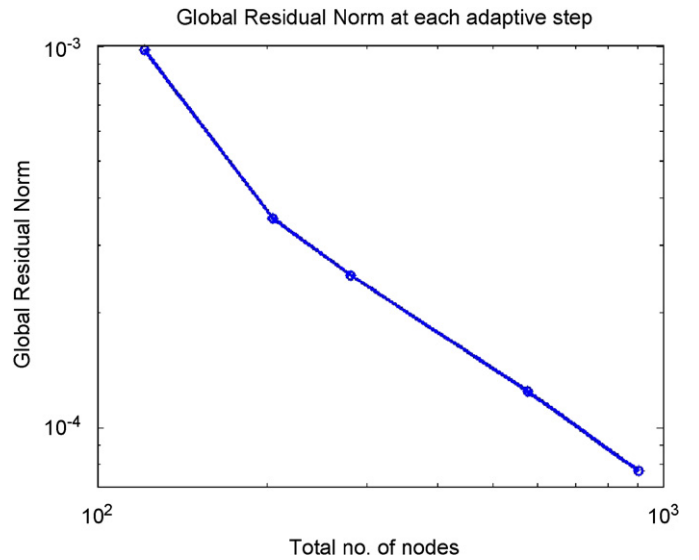


Fig. 17. Estimated global residual norm at each step in the adaptive analysis using LS-RPCM.

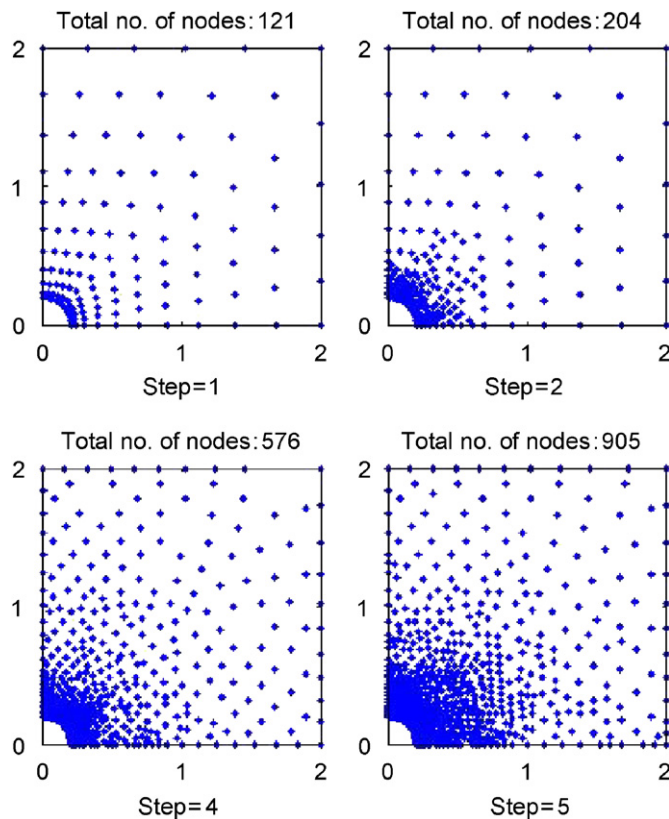


Fig. 16. Nodal distributions at 1st, 2nd, 4th and final step in the adaptive analysis using LS-RPCM.

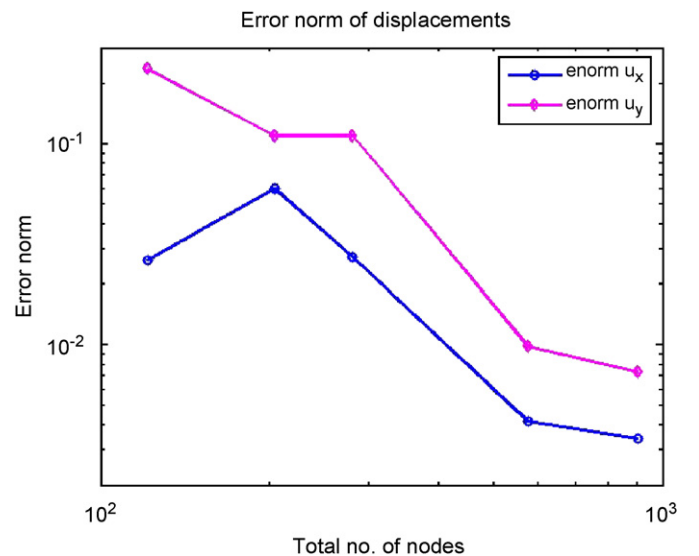


Fig. 18. Error norm of the displacements at each step.

where φ is the stress function, G is the shear modulus of the bar and θ is the twisted angle. The relationship of the stresses and stress function is given as

$$\tau_{xz} = \frac{\partial \varphi}{\partial y}; \quad \tau_{yz} = -\frac{\partial \varphi}{\partial x}. \quad (30)$$

Torsion problem is a Dirichlet problem, the boundary condition is known as

$$\frac{\partial \varphi}{\partial y} \frac{\partial y}{\partial s} + \frac{\partial \varphi}{\partial x} \frac{\partial x}{\partial s} = \frac{\partial \varphi}{\partial s} = 0. \quad (31)$$

The above equation shows the stress function φ must be constant along the boundary of the cross section, and φ is arbitrarily chosen as zero for this problem.

A uniform triangular cross section bar is studied in this example and the twist angle is given as $\theta = 1$. The dimensions of the problem are given in Fig. 9. The analytical solution of this problem is given as

$$\varphi = -G\theta \left[\frac{1}{2}(x^2 + y^2) - \frac{1}{2a}(x^3 - 3xy^2) - \frac{2}{27}a^2 \right]. \quad (32)$$

To study the approximated convergent rate of the error norm for φ of the LS-RPCM and the RPCM, four sets of regular nodal distribution are used (see Fig. 9). It is shown in Fig. 10 that the convergent rate of the error norm for φ of the RPCM and the LS-RPCM is about the same, $R = 2.95$. The accuracy of the LS-RPCM is slight higher than the RPCM.

The same torsion problem is also analysed using an elliptic bar. To examine the numerical performance of the RPCM and the LS-RPCM for the scattered nodes, the bar is modelled by 511 nodes irregularly distributed in the problem domain as shown in Fig. 11. The analytical solution of the problem is now known as a second-order

polynomial

$$\varphi = -\frac{a^2 b^2}{a^2 + b^2} G\theta \left(\frac{x^2}{a^2} + \frac{y^2}{b^2} - 1 \right). \quad (33)$$

As the RPIM shape function (Eq. (5)) is able to reproduce the second-order polynomial function [5,6], the accuracy for both the RPCM and the LS-RPCM is up to the machine accuracy as listed in Table 2.

The purpose of this example is not to emphasize on the reproductivity of the RPIM shape function for the polynomial function. Rather, we would like to point out that the RPCM based on local nodes can achieve excellent accuracy even for scattering nodes, if the Neumann boundary condition is not involved. In this example with only Dirichlet boundary condition being involved, the RPCM is able to obtain good result without any stabilization measure. Note that, the LS-RPCM can also

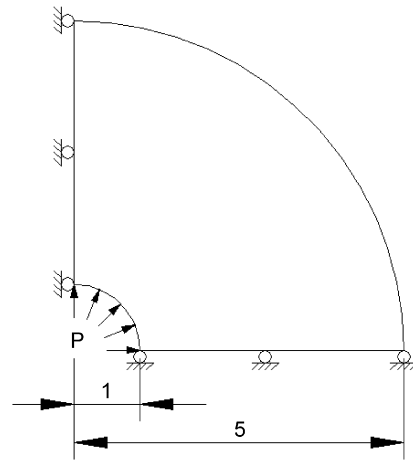


Fig. 20. Quarter of the model of a cylinder subjected to internal pressure.

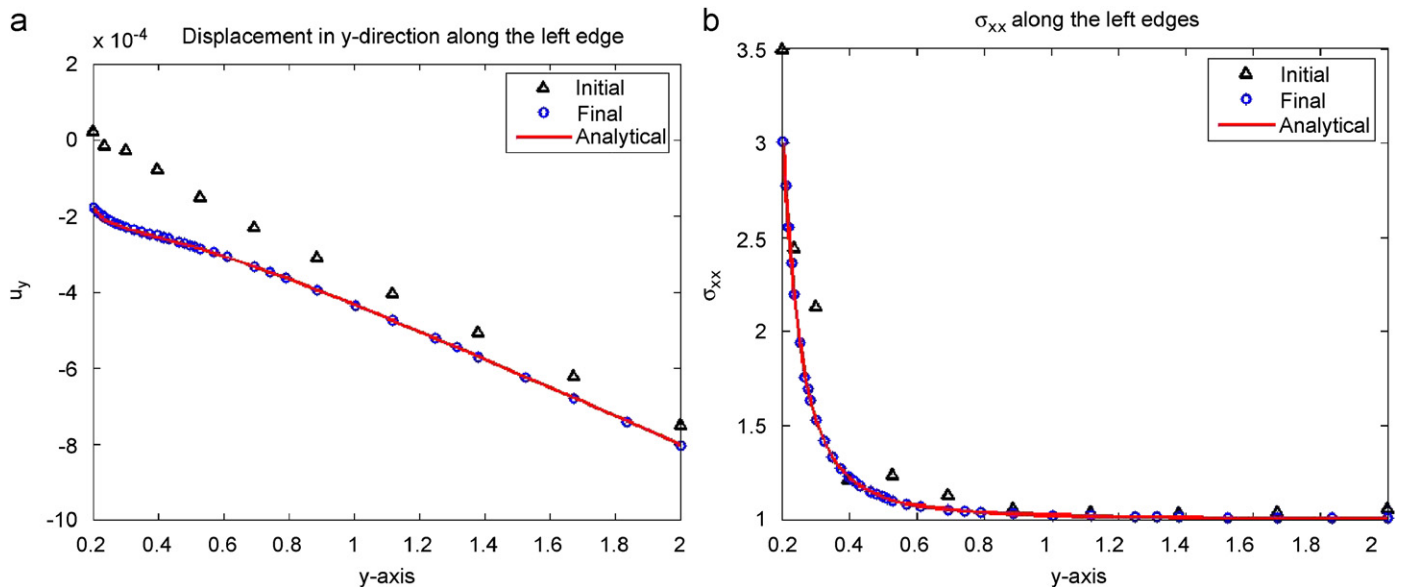


Fig. 19. (a) Displacements in y -direction and (b) normal stresses σ_{xx} along the left edge at first and final step.

achieve very good accuracy for the Dirichlet problem as well.

6.3. Example 3

In this example, a benchmark plane strain solid mechanics problem is studied to reveal the instability problem encountered by the RPCM. An infinite plate with circular hole is subjected to a unit traction P in the horizontal direction. Due to the symmetry, only quarter of the problem is modelled as shown in Fig. 12. Symmetric boundary condition is imposed along the left and bottom edges. The geometry and material properties are given as: $a = 0.2$, $b = 2.0$, Young's modules, $E = 1 \times 10^3$ and Poisson's ratio, $\nu = 0.3$. The governing equations of elastostatics problem are well known as

$$\sigma_{ij,j} + b_i = 0 \text{ in } \Omega. \tag{34}$$

Dirichlet boundary conditions are given as

$$u_i = \bar{u}_i \text{ on } \Gamma_u, \tag{35}$$

and Neumann boundary conditions are given as

$$\sigma_{ij}n_j = t_i \text{ on } \Gamma_t. \tag{36}$$

The analytical solution of this problem can be found in Ref. [48].

To demonstrate the instability problem of the RPCM, two similar sets of nodal distribution are used (see Fig. 13). Model A is made up by 435 nodes. Eighteen nodes are added into Model A to form Model B. Although there are

only 18 nodes that are different between Model A and Model B, the results obtained by the RPCM based on these two models are tremendously different. The numerical solutions of the displacements and the stresses along the left edge are plotted in Fig. 14. It is clear that the solution computed by the RPCM is unstable. Both the solutions of displacements and stresses for Model A and Model B are significantly different. Compared to the RPCM, the

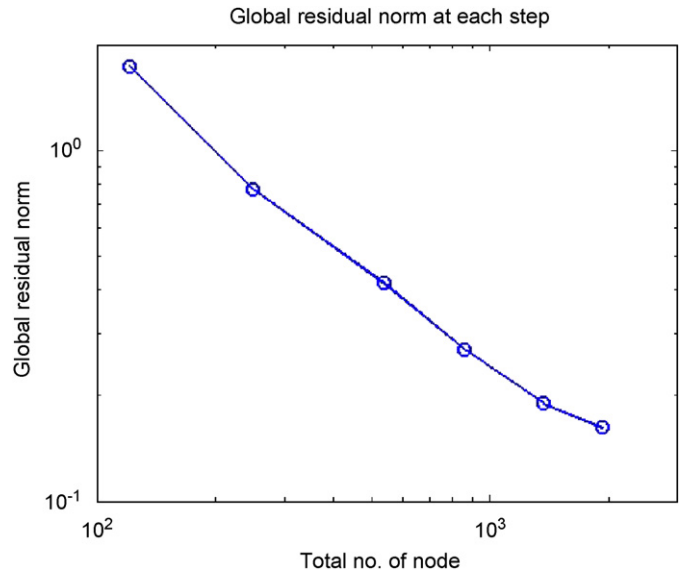


Fig. 22. Estimated global residual norm at each step.

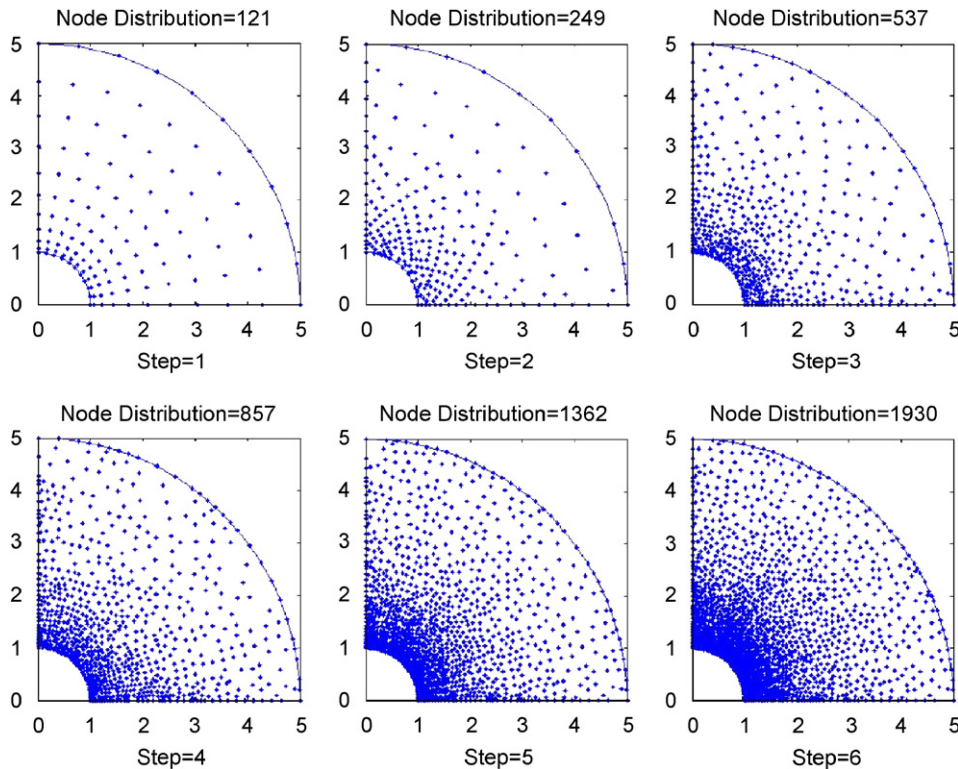


Fig. 21. Nodal distributions at each adaptive step.

solution obtained by the LS-RPCM is very stable and much more accurate.

In the RPCM formulation procedure, the boundary conditions are fully satisfied on the boundary point. Rather, in our present least-square procedure, the boundary conditions are satisfied in the least-square sense. In this example, $\sigma_{yy} = 0$ is the Neumann boundary condition along the top edge. From Fig. 15, one can observe that the boundary condition along the top edge ($\sigma_{yy} = 0$) is fully satisfied by the RPCM at the boundary nodes *only*. We notice that the value of σ_{yy} is frustrating other than the nodes (still along the top edge), oscillation is observed. Except at the boundary nodes, the interpolation value of σ_{yy} can vary significantly from zero (the exact condition) along the top edge as shown in Fig. 15. In the present

formulation, the least-square procedure provides a kind of “relaxation” effect upon the strong formulation against the “strong” requirement of the boundary conditions. Good

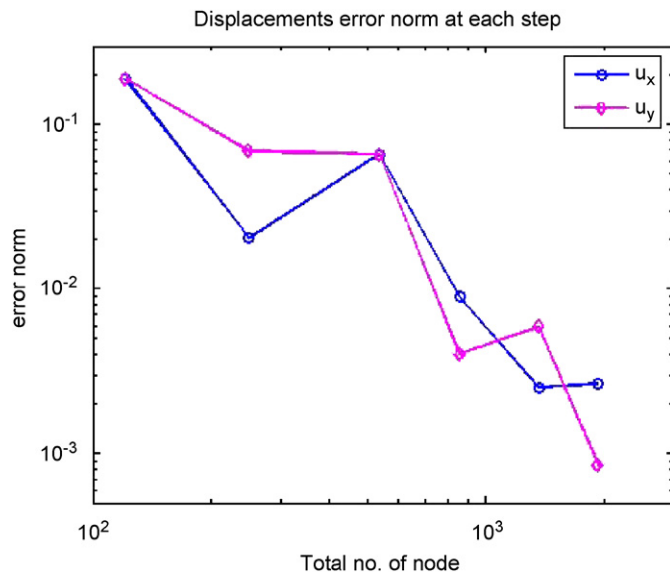


Fig. 23. Error norm of the displacements at each step.

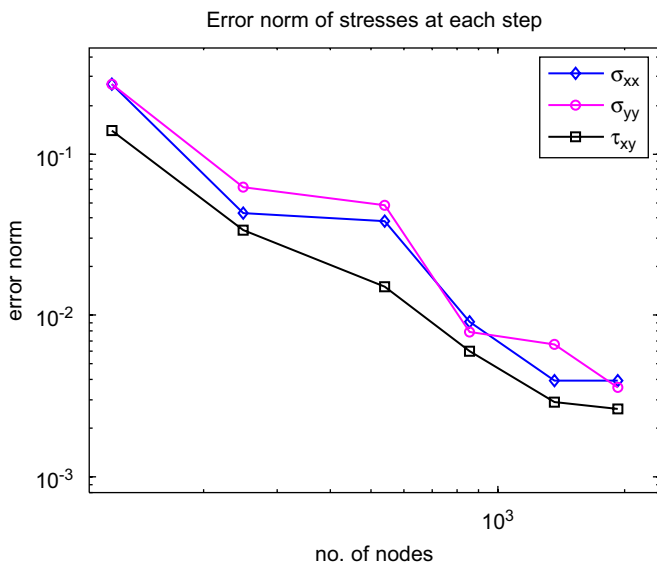


Fig. 24. Error norm of the stresses at each step.

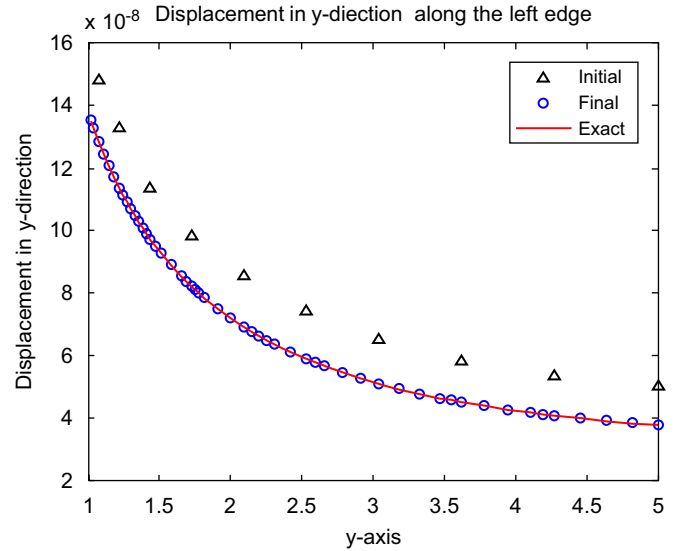


Fig. 25. (a) Displacements in y-direction and (b) normal stresses σ_{xx} along the left edge at first and final step.

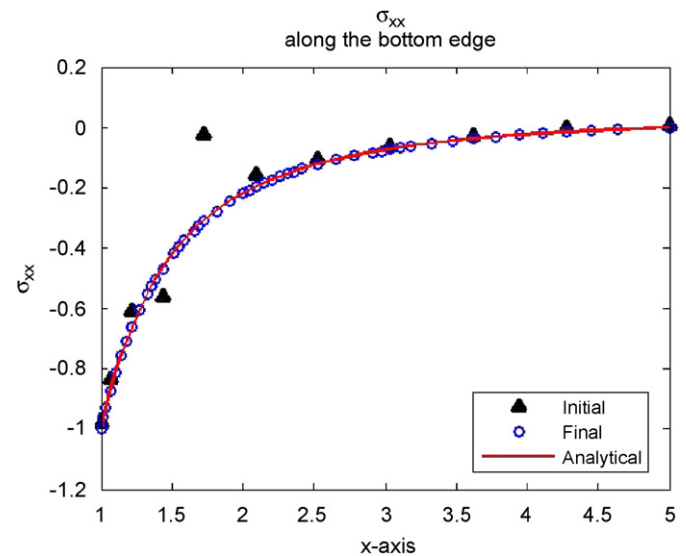


Fig. 26. (a) Displacements in y-direction and (b) normal stresses σ_{xx} along the left edge at first and final step.

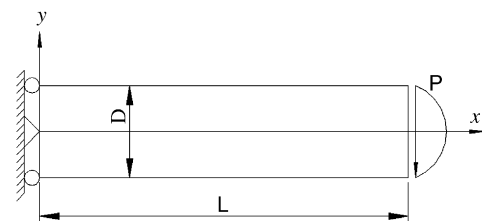


Fig. 27. Cantilever beam subjected to a parabolic shear stress at the right end.

approximated solutions can be obtained by the LS-RPCM as shown in Fig. 15.

As the stability is restored, the LS-RPCM is incorporated then with the residual based error estimator to performance adaptive analysis subsequently. The adaptive analysis started with 121 nodes irregularly distributed in the problem domain. Sixteen nodes are used for constructing the shape functions. The local refinement coefficient is predefined as $\kappa_l = 0.1$ and the global residual tolerance is set as $\kappa_g = 0.1$. The adaptive analysis ended at 5th step with 905 nodes irregularly distributed in the problem domain as shown in Fig. 16.

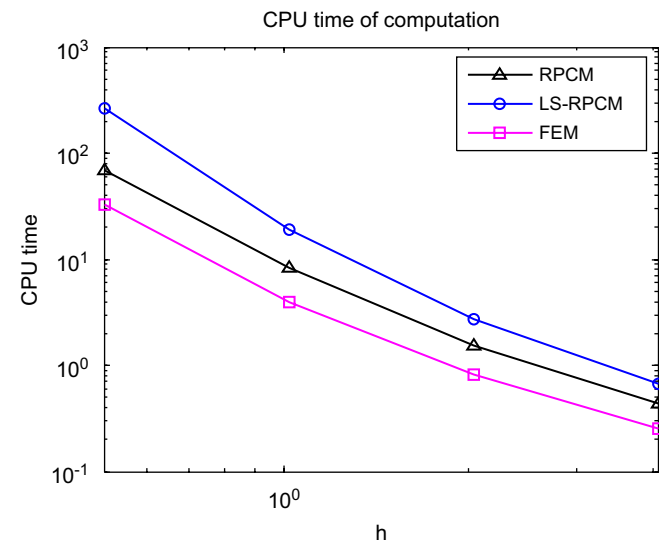


Fig. 28. Comparison of CPU times among RPCM, LS-RPCM and FEM against mesh size h .

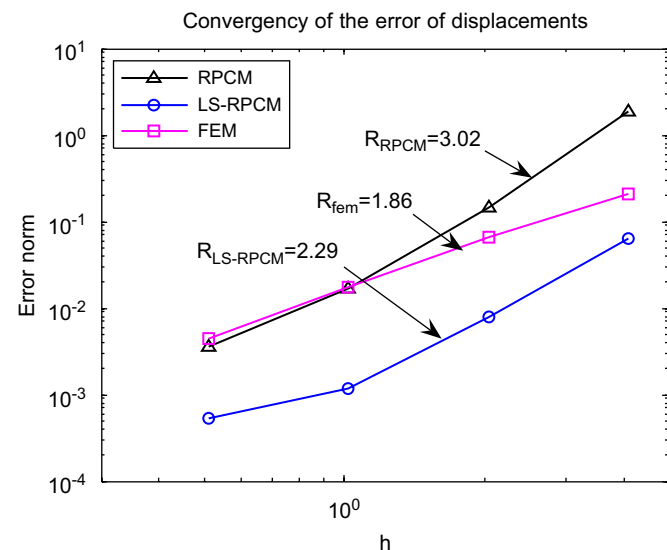


Fig. 29. Comparison of error norm of displacements among RPCM, LS-RPCM and FEM against mesh size h .

The estimated global residual norm at each adaptive step is plotted in Fig. 17. One can notice that the estimated global residual norm is gradually reduced at each adaptive step. Excellent stability of the LS-RPCM is demonstrated (Fig. 18). The error norms of the displacements in x - and y -directions are also plotted in Fig. 18. For reference purpose, the displacements and stresses along the bottom edge are plotted at initial and final steps as shown in Fig. 19. It is evidently clear that the accuracy of both displacements and stresses have been greatly improved through our effective adaptive scheme.

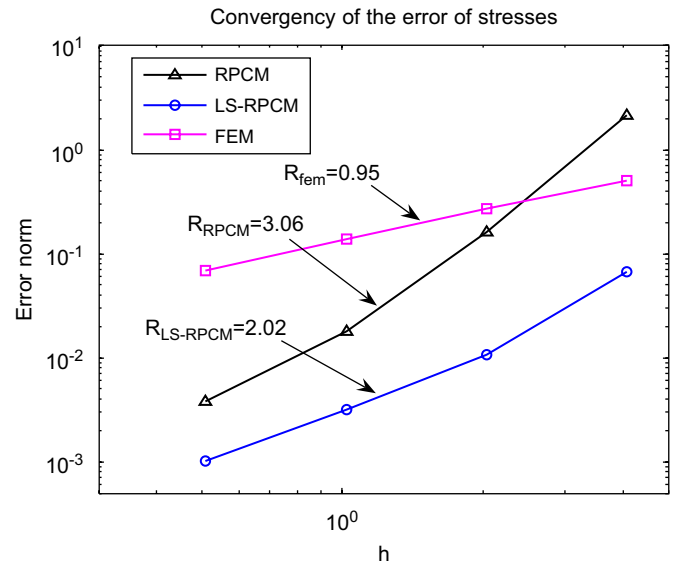


Fig. 30. Comparison of error norm of stresses among RPCM, LS-RPCM and FEM. For RPCM and LS-RPCM, stresses are sampled at the node; for FEM, stresses are sampled at the centre of the element.

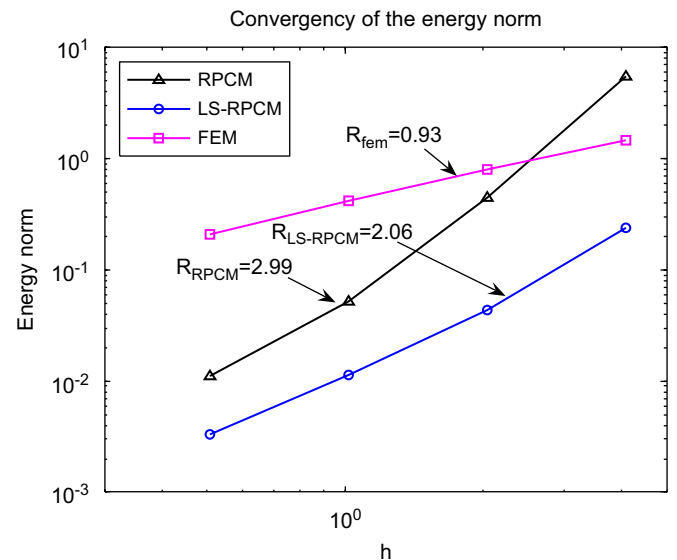


Fig. 31. Comparison of energy norm among RPCM, LS-RPCM and FEM.

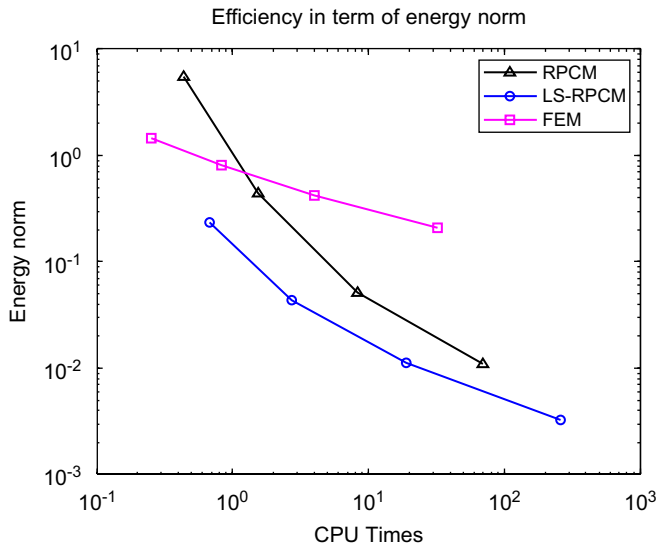


Fig. 32. Comparison of efficiency in term of energy norm among RPCM, LS-RPCM and FEM.

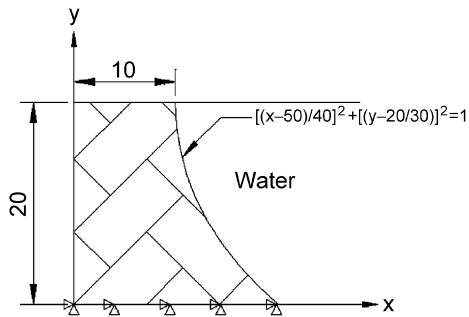


Fig. 33. A reservoir fully filled with water.

6.4. Example 4

The fourth example is a thick wall cylinder subject to an internal pressure. The material properties and geometries are given as: internal radius $a = 1$, external radius $b = 5$, Young's modulus $E = 1 \times 10^7$, Poisson's ratio $\nu = 0.3$ and internal pressure $P = 1$ MPa. The analytical solution of this problem is well known and can be found in Ref. [49].

As this problem is symmetric, only quarter of the problem is modelled as shown in Fig. 20. Symmetric

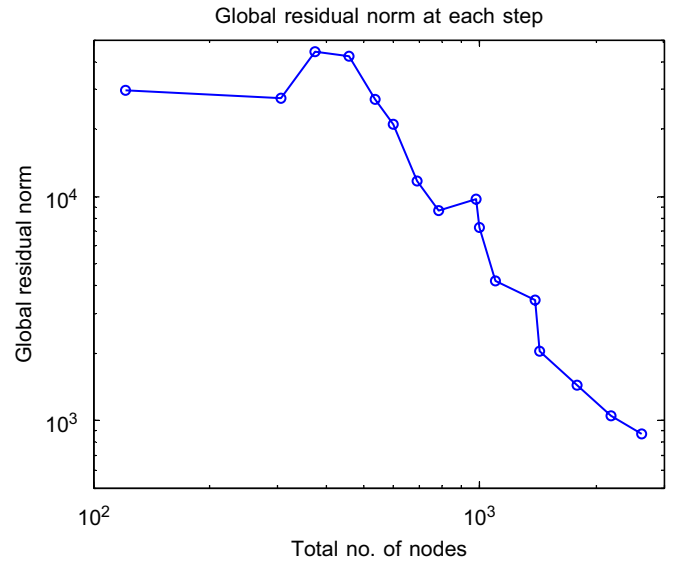


Fig. 35. Estimated global residual norm at each adaptive step.

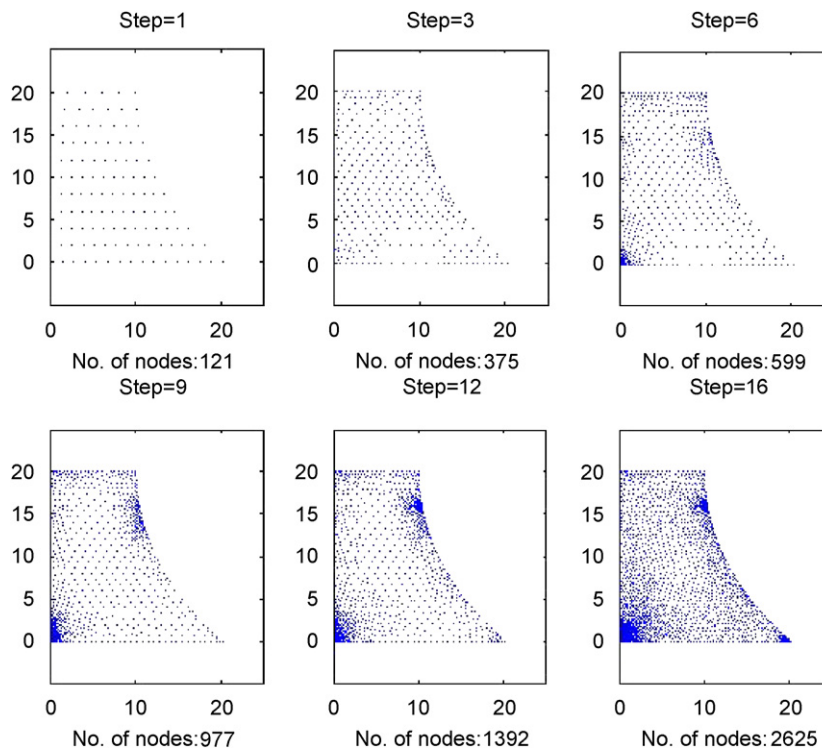


Fig. 34. Nodal distributions at 1st, 3rd, 6th, 9th, 12th, 16th step.

boundary condition is imposed along the left and bottom edges. In this example, only 15 nodes are used for constructing the shape functions. The local refinement coefficient is predefined as $\kappa_l = 0.1$ and the global residual tolerance is set as $\kappa_g = 0.025$. The adaptive analysis is started with 121 regularly distributed nodes in the domain and stop at the 6th step with 1930 nodes irregularly distributed in domain, as shown in Fig. 21. The estimated global residual norm at each step is plotted in Fig. 22. The error norm of the displacements has been greatly reduced from 19.08% for both displacements in x -direction and y -direction to 0.27% and 0.09%, respectively as shown in Fig. 23. The error norm of the stresses has also been reduced dramatically as shown in Fig. 24.

The displacements and stresses along the left edge are plotted and compared with analytical solution as shown in Figs. 25 and 26. These plots show the adaptive scheme has effectively refined the critical domain based on error estimator and hence the solutions are improved. The numerical solutions of the displacements and stresses at the final steps are in very good agreement with the analytical solutions.

6.5. Example 5

To examine the computational efficiency of the LS-RPCM, a bench mark elastostatics plane stress problem is studied. A cantilever beam with unit thickness is subjected

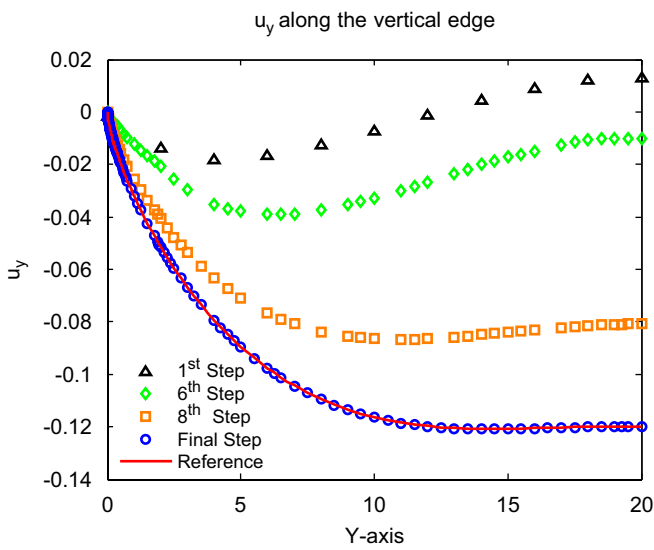


Fig. 36. Displacement in y -direction at 1st, 6th, 8th and final along the vertical edge.

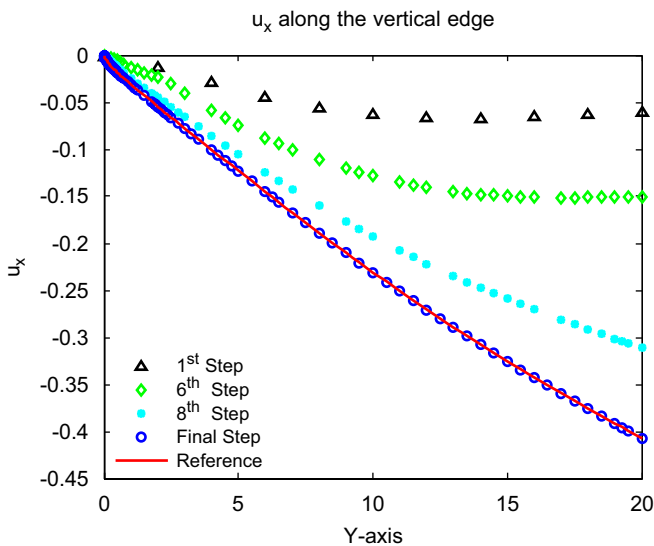


Fig. 37. Displacement in x -direction at 1st, 6th, 8th and final along the vertical edge.

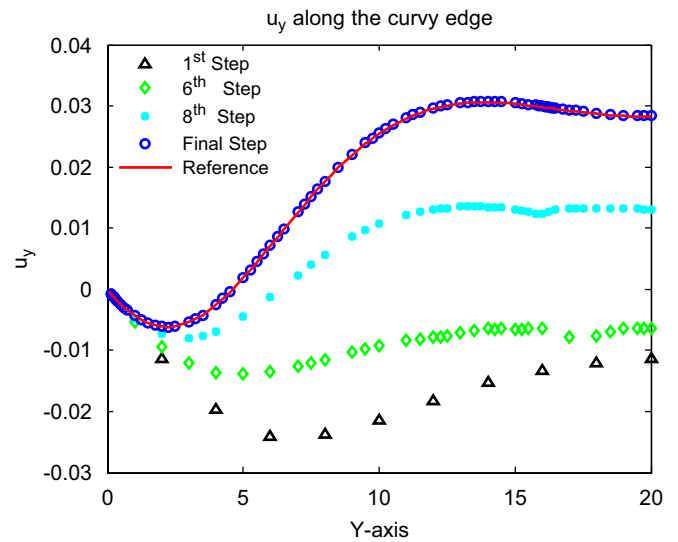


Fig. 38. Displacement in y -direction at 1st, 6th, 8th and final along the curvy edge.

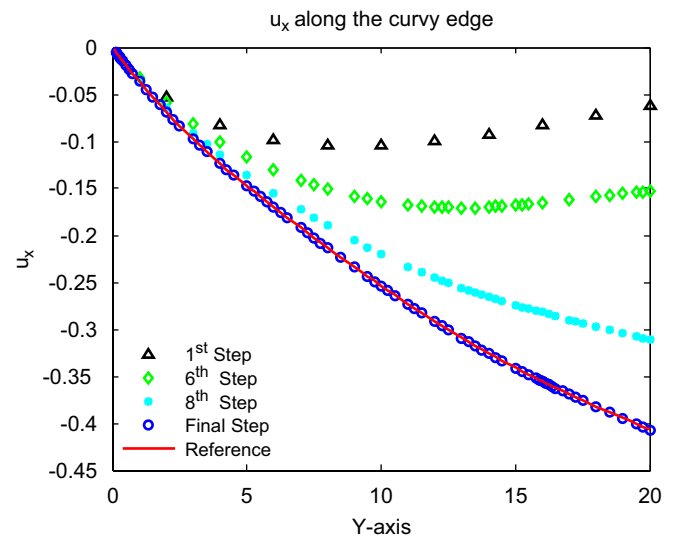


Fig. 39. Displacement in x -direction at 1st, 6th, 8th and final along the curvy edge.

to a parabolic shear stress at the right end as shown in Fig. 27. The material properties and geometrics are given as: Young’s modulus $E = 3 \times 10^7$, Poisson’s ratio $\nu = 0.3$, length of cantilever $L = 48.0$ m and the height $H = 12.0$ m. The loading is known as $\tau_{xy} = -(P/2I)(H^2/4 - y^2)$, where I is moment of inertial of the cross section of cantilever and $P = 1000$ N. Analytical solution can be found in Ref. [48].

In this example, four sets of regular nodal distribution: 5×11 , 9×21 , 17×41 and 33×81 , are used. Sixteen

supporting nodes are used for constructing the shape functions. The computational time required for each model is plotted in Fig. 28 and compared with the RPCM and the FEM. Convergent rate of the error norms of displacements, stresses and energy norm are also compared as shown in Figs. 29–31. Their efficiencies in term of the energy norm are also plotted in Fig. 32.

From Fig. 28, one can observe that the computational time required for the LS-RPCM is higher than the RPCM

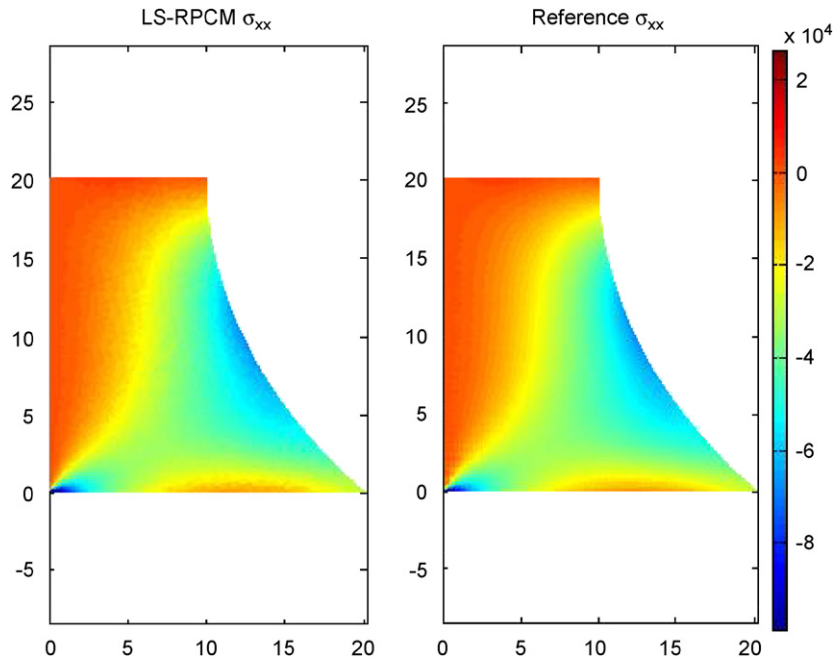


Fig. 40. Contour plot of the normal stress σ_{xx} .

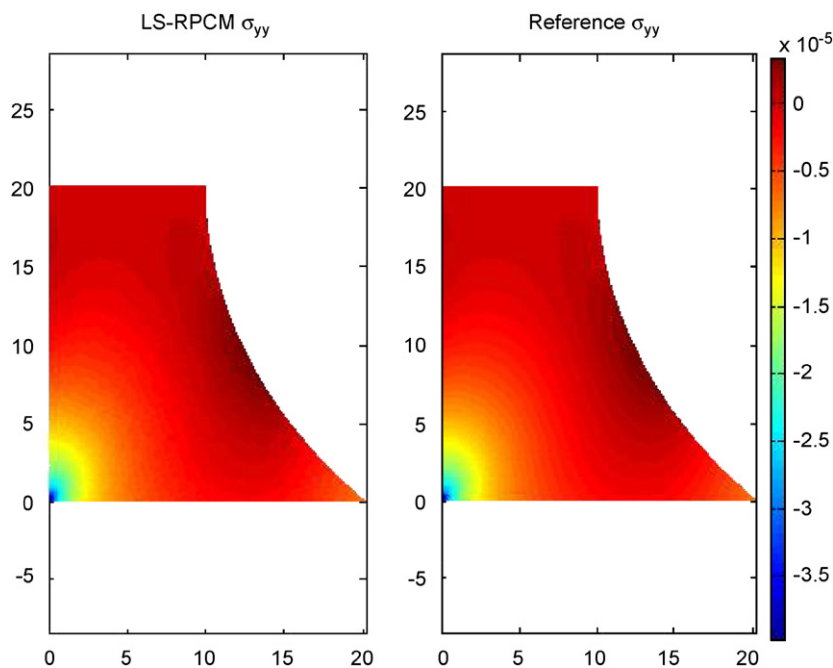


Fig. 41. Contour plot of the normal stress σ_{yy} .

and the FEM. It is due to the use of the least-square procedure in the LS-RPCM. The convergent rates of the error norm of displacements and energy norm are approximately about 2.29 and 2.06, respectively. The accuracy of the LS-RPCM for the displacements is comparable with FEM as shown in Fig. 29. In term of the accuracy of the stresses and the convergent rate of the energy norm, the LS-RPCM performs better than FEM as shown in Figs. 30 and 31. The efficiency rate in term of energy norm of the LS-RPCM is also the best among these three methods. Although the RPCM seems performing well in the regular nodal distribution in Figs. 29–31, the instability issue is still fatal shortcoming that prohibits the RPCM from being used in adaptive analysis.

6.6. Example 6

In this example, the wall of a reservoir fully filled with water is investigated. The geometry of the wall is irregular as given in Fig. 33. The material properties of the wall are given as Young’s Modulus $E = 1 \times 10^7$ and Poisson’s ratio $\nu = 0.3$. The bottom of the wall is fixed and the curvy edge of the wall is subjected to a hydrostatic pressure $P = -9800(H - y)$ MPa.

As analytical solution is not available in this case, a very fine mesh (59,400 linear triangular elements) FEM solution will be considered as our references solution. The problem is initially modelled by 121 nodes as shown in Fig. 34. The local refinement coefficient is predefined as $\kappa_l = 0.1$ and the global residual tolerance is set as $\kappa_g = 0.025$. The adaptive analysis ended at 16th step with 2625 nodes irregularly distributed in the domain.

The final nodal distribution in Fig. 34 has shown that the residual based error estimator has effectively identified the

high stress regions. The estimated global residual norm is gradually reduced through out the adaptive process as shown in Fig. 35. From Figs. 36–39, the numerical solutions of the displacements have been improved greatly through the adaptive analysis. The contour plots for stresses are also given in Figs. 40–42, and the final solutions of stresses are in very well agreement with the reference solutions. The stresses along the curvy edge are also plotted and compared with references solutions in Fig. 43, and it shows the numerical solutions of the stresses very tally with reference solutions as well.

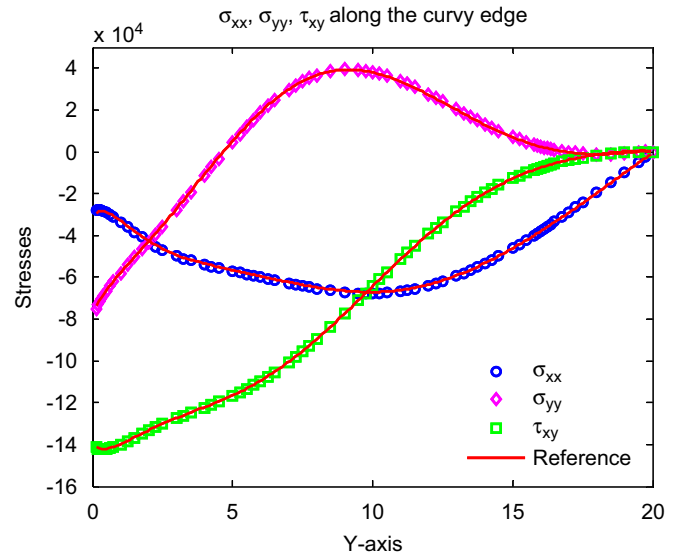


Fig. 43. The stresses along the curvy edge.

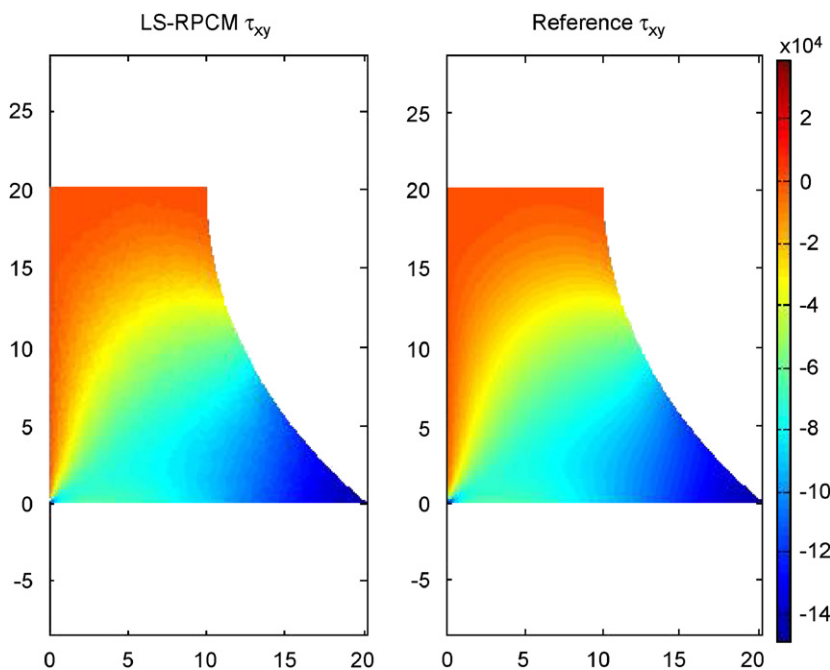


Fig. 42. Contour plot of the shear stress τ_{xy} .

7. Discussions

As shown in the first two examples, the RPCM has exhibited its excellent numerical performance for one-dimensional problem and the Dirichlet problem. The first numerical example has shown the RPCM a stable method for problem with solution of high gradient in one-dimensional space. No instability takes place during the adaptation. Results have also shown that the residual based error estimator is robust and able to identify the high gradient region. Example 2 shows the RPCM can also be used for solving Dirichlet problem. Torsion problem with irregular geometry and irregular nodal distribution can be solved with good accuracy.

However, while the Neumann boundary condition is involved, instability is a fatal shortcoming of the RPCM as clearly illustrated in Example 3. In Examples 3, 4 and 6, the LS-RPCM has been successfully implemented for the adaptive analysis. Stable and accurate results can be obtained. The computational efficiency of the LS-RPCM is also studied and compared with the FEM and the RPCM in the Example 5. Having additional collocation points on the boundary have been proven effectively restores the stability in these examples. We have also tried to introduce more collocation points in the problem domain, and we found that it may help but it is not necessary.

8. Concluding remarks

In this paper, a least-square radial point collocation method (LS-RPCM) is proposed. The notorious instability problem encountered by the conventional RPCM is resolved by the proposed least-square procedure. By having additional collocation point on the boundary, it provides a “relaxation” effect that reduces the “strong” requirement for the boundary condition in the strong formulation. Number of numerical examples has shown that stable solutions can be obtained through the simple and yet effective least-square procedure. As stable solution can be achieved, the LS-RPCM has well demonstrated its advantages in adaptive analysis. The residual based error estimator is also shown robust and efficient. Refinement procedure using Delaunay diagram is demonstrated as a simple and yet a versatile procedure to insert additional nodes during the refinement process. Numerical examples have shown the LS-RPCM not only obtained stable and accurate result but also successfully implemented for adaptive analysis which conventional RPCM cannot perform.

References

- [1] Liu GR, Liu MB. Smoothed particle hydrodynamics: a meshfree particle method. World Scientific; 2003.
- [2] Lucy L. A numerical approach to testing the fission hypothesis. *Astron J* 1977;82:1013–24.
- [3] Gingold R, Monaghan J. Smoothed particle hydrodynamics: theory and application to nonspherical stars. *Monthly Notices R Astron Soc* 1977;181:375–89.
- [4] Belyschko T, Krongauz Y, Organ D, Fleming M, Krysl P. Meshless methods: an overview and recent developments. *Comput Methods Appl Mech Eng* 1996;139:3–47.
- [5] Liu GR. Meshfree method: moving beyond the finite element method. CRC Press; 2002.
- [6] Liu GR, Gu YT. An introduction to meshfree methods and tier programming. Springer; 2005.
- [7] Onate E, Perazzo F, Miquel J. A finite point method for elasticity problems. *Comput Struct* 2001;79:2153–63.
- [8] Liszka TJ, Duarte C, Tworzydło WW. hp-Meshless cloud method. *Comput Methods Appl Mech Eng* 1996;139:263–88.
- [9] Cheng M, Liu GR. A novel finite point method for flow simulation. *Int J Numer Methods Fluids* 2002;39(12):1161–78.
- [10] Liszka T, Orkisz J. Finite difference methods of arbitrary irregular meshes in non-linear problems of applied mechanics. In: *Proceedings of 4th international conference on structural mechanics in reactor technology*, San Francisco, USA, 1977.
- [11] Liszka T, Orkisz J. Finite difference method at arbitrary irregular grids and its application in applied mechanics. *Comput Struct* 1979;11:88–95.
- [12] Girault V. Theory of a finite difference method on irregular networks. *SIAM J Numer Anal* 1974;11(2):260–82.
- [13] Pavlin V, Perrone N. Finite difference energy techniques for arbitrary meshes applied to linear plate problems. *Int J Numer Methods Eng* 1979;14(5):647–64.
- [14] Liu X, Liu GR, Tai K, Lam KY. Radial basis interpolation collocation method for the solution of partial differential equations. *Comput Math Appl* 2005;50:1425–42.
- [15] Atluri SN, Zhu T. A new meshless local Petrov–Galerkin (MLPG) approach in computational mechanics. *Comput Mech* 1998;22:117–27.
- [16] Belyschko T, Lu YY, Gu L. Element-free Galerkin method. *Int J Numer Methods Eng* 1994;37:229–56.
- [17] Liu WK, Jun S. Multiple-scale reproducing kernel particle methods for large deformation problems. *Int J Numer Methods Eng* 1998;41:1339–62.
- [18] Liu GR, Gu YT. A local radial point interpolation method (LRPIM) for free vibration analyses of 2-D solids. *J Sound Vibr* 2001;246:29–46.
- [19] Liu GR, Zhang GY, Gu YT, Wang YY. A meshfree radial point interpolation method (RPIM) for three-dimensional solids. *Comput Mech* 2005;36:421–30.
- [20] Liu GR, Gu YT. A point interpolation method for two-dimensional solids. *Int J Numer Methods Eng* 2001;50:937–51.
- [21] Liu GR, Zhang GY, Dai KY. A linearly conforming point interpolation method (LC-PIM) for 2D solid mechanics problems. *Int J Comput Methods* 2007;2:645–65.
- [22] Li Y, Liu GR, Luan MT, Dai KK, Zhong ZH, Li GY, et al. Contact analysis for solids based on linearly conforming RPIM. *Comput Mech* 2007;39(4):537–54.
- [23] Wang JG, Liu GR. On the optimal shape parameters of radial basis functions. *Comput Methods Appl Mech Eng* 2002;191:21–6.
- [24] Liu GR, Gu YT. A meshfree method: meshfree weak–strong form method for 2-D solids. *Comput Mech* 2003;33:2–14.
- [25] Liu GR, Wu YL, Ding H. Meshfree weak–strong (MWS) form method and its application to incompressible flow problems. *Int J Numer Methods Fluids* 2004;46:1025–47.
- [26] Kovacevic I, Sarler B. Solution of a phase-field model for dissolution of primary particles in binary aluminium alloys by an r-adaptive meshfree method. *Mater Sci Eng, A* 2005;413/414:423–8.
- [27] Liu GR, Kee BBT, Lu C. A stabilized least-squares radial point collocation method (LS-RPCM) for adaptive analysis. *Comput Methods Appl Mech Eng* 2006;195:4843–61.
- [28] Liu GR, Kee BBT. An adaptive meshfree method based on regularized least-squares formulation. In: *13th international conference*

- on computational and experimental engineering and sciences (ICCES), Chennai, India, 2005.
- [30] Courant R, Friedrichs KO, Lewy H. Über die partiellen differenzgleichungen der mathematischen Physik. *Math Ann* 1928;100:32–74.
- [31] Kansa EJ. Multiquadrics—a scattered data approximation scheme with applications to computational fluid-dynamics I&II. *Comput Math Appl* 1990;19(8/9):127–61.
- [32] Kansa EJ, Hon YC. Circumventing the ill-conditioning problem with multiquadric radial basis functions: application to elliptic partial differential equations. *Comput Math Appl* 2000;39:123–37.
- [33] Wu Z. Positive definite radial basis function with compact support. *Adv Comput Math* 1995;4:283–92.
- [34] Fedoseyev AI, Friedman MJ, Kansa EJ. Improved multiquadric method for elliptic partial differential equations via PDE collocation on the boundary. *Comput Math Appl* 2002;43:439–55.
- [35] Chen W, Tanaka M. New insights in boundary-only and domain-type RBF methods. *Int J Nonlinear Sci Numer Simul* 2000;1(3):145–51.
- [36] Liu X, Liu GR, Tai K, Lam KY. Radial basis point interpolation collocation method for 2-d solid problem. In: *Proceedings of the 2nd international conference on structural stability and dynamics*, Singapore, December 16–18, 2002, p. 35–40.
- [37] Liu X, Liu GR, Tai K, Lam KY. Radial point interpolation collocation method (RPICM) for the solution of nonlinear Poisson problems. *Comput Mech* 2005;36(4):298–306.
- [38] Divo E, Kassab AJ. An efficient localized radial basis function meshless method for fluid flow and conjugate heat transfer. *ASME J Heat Transfer* 2007;129:124–36.
- [39] Šarler B, Vertnik R. Meshfree explicit local radial basis function collocation method for diffusion problems. *Comput Math Appl* 2006;51:1269–82.
- [40] Zhang X, Liu XH, Song KZ, Lu MW. Least-squares collocation meshless method. *Int J Numer Methods Eng* 2001;51:1089–100.
- [41] Zienkiewicz OC, Taylor RL. *The finite element method*, vol. 1, 1989, vol. 2, 1992. New York: McGraw-Hill; 1992.
- [42] Franke R. Scattered data interpolation: test of some methods. *Math Comput* 1982;38(157):181–200.
- [43] Hardy RL. Theory and applications of multiquadrics-Biharmonic method (20 years of discovery 1968–1988). *Comput Math Appl* 1990;19(8/9):163–208.
- [44] Golberg MA, Chen CS, Karur SR. Improved multiquadrics approximation for partial differential equations. *Eng Anal Boundary Elem* 1996;18:9–17.
- [45] Hon YC, Lu MW, Xue WM, Zhu YM. Multiquadric method for the numerical solution of a biphasic mixture model. *Appl Math Comput* 1997;88:153–75.
- [46] Franke C, Schaback R. Solving partial differential equations by collocation using radial basis functions. *Appl Math Comput* 1998;93:73–82.
- [47] Liu GR, Han X. *Computational inverse techniques in non-destructive evaluation*. CRC Press; 2003.
- [48] Timoshenko SP, Goodier JN. *Theory of elasticity*. New York: McGraw-Hill; 1970.
- [49] Cook DR, Yong WC. *Advanced mechanics and materials*. Prentice-Hall; 1998.
- [51] Onate E, Idelsohn S, Zienkiewicz OC, Taylor RL. A finite point method in computational mechanics. Application to convection transport and fluid flow. *Int J Numer Methods Eng* 1996;39(22):3839–66.
- [52] Sadat H, Prax C. Application of the diffuse approximation for solving fluid flow and heat transfer problems. *Int J Heat Mass Transfer* 1996;39(1):214–8.
- [53] Wang JG, Liu GR. A point interpolation meshless methods based on radial basis functions. *Int J Numer Methods Eng* 2002;54:1623–48.
- [55] Xu G, Liu GR. Development of irregular-grid finite difference method (IFDM) for governing equation in strong-form. *WSEAS Trans Math* 2006;5(10):1117–22.